Pharmacological or genetic inhibition of *Scn9a* protects beta-cells while reducing insulin secretion in type 1 diabetes.

Peter Overby[1], Sophia Provenzano[1], Natalie S. Nahirney[1], Xiao-Qing Dai[2], WenQing Grace Sun[1], Yi Han Xia[1], Jiashuo Aaron Zhang[1], Haoning Cen[1], Søs Skovsø[1], Jelena Kolic[1], Patrick E. MacDonald[2], James D. Johnson[1]*

[1] Diabetes Research Focus Team, Life Science Institute, Department of Cellular & Physiological Sciences, University of British Columbia, Vancouver, BC.

[2] Li Ka Shing Centre, Department of Pharmacology and Alberta Diabetes Institute, University of Alberta, Edmonton, Alberta.

Author Contributions:

P.O. Co-conceived experiments, conducted experiments, analyzed data and wrote the manuscript.

S.P. Conducted *in vivo* and *in vitro* experiments.

N.S.H. Conducted *in vivo* and *in vitro* experiments.

X-D. D. Designed, performed, and analyzed electrophysiological studies.

W.G.S. Conducted experiments (insulin quantification)

Y.H.X. Performed bioinformatic analysis and data visualization (mouse RNAseq analysis)

J.A.Z. Performed bioinformatic analysis and data visualization (human and mouse scRNA analysis)

H.C. Supervised bioinformatic analysis and data visualization.

S.S Supervised *in vivo* work

J.K. Conducted experiments, supervised work, edited manuscript.

P.M. Supervised work, edited manuscript.

J.D.J. Conceived studies, supervised/guarantees the work, edited manuscript. *Corresponding author

Acknowledgements: The thank members of the Johnson and MacDonald labs, as well as members of the JDRF Centre of Excellence for helpful discussions. We thank the Human Organ Procurement and Exchange (HOPE) program and Trillium Gift of Life Network (TGLN) for their work in procuring human donor pancreas for research, and James Lyon, Nancy Smith and Dr. Jocelyn Manning Fox (Alberta) for their efforts in human islet isolation. We especially thank the organ donors and their families for their kind gift in support of diabetes research.

Funding: This project was supported by a JDRF Project Grant and a Bridge Grant from CIHR to J.D.J. We also acknowledge the core support through the JDRF Centre of Excellence (3-COE-2022-1103-M-B). Work in Edmonton was supported by a Foundation Grant (148451) from CIHR to P.E.M. P.E.M. holds the Tier 1 Canada Research Chair in Islet Biology.

Abstract

Pancreatic β-cells are critical for systemic glucose homeostasis, and most of them undergo cell death during the pathogenesis of type 1 diabetes. We previously showed that a Na^+ channel inhibitor, carbamazepine, could protect β-cells *in vitro* and *in vivo*. Here, we confirmed the effects of carbamazepine and other Na^+ channel inhibitors on human islets and focused on the specific role of the Na^+ channel gene, *Scn9a* (Nav1.7), in β-cell function and survival. Because *Scn9a* can be found in multiple human and mouse islet cell types, we generated a β-cell specific knockout of *Scn9a* on the non-obese diabetic (NOD) background. We crossed an *Scn9a*$^{flox/flox}$ allele onto the *Ins1*^{Cre} knock-in mouse line resulting in the following genotypes: knockout (NOD.*Ins1*^{Cre};*Scn9a*$^{flox/flox}$), heterozygous (NOD.*Ins1*^{Cre};*Scn9a*$^{flox/wt}$), and wildtype littermate controls (NOD.*Ins1*^{Cre};*Scn9a*$^{wt/wt}$). We observed near complete ablation of Na^+ currents in knockout β-cells, and intermediate Na^+ currents in the heterozygotes. Insulin secretion in response to 15 mM glucose, but not lower concentrations, was significantly reduced from NOD.*Ins1*^{Cre};*Scn9a*$^{flox/flox}$and NOD.*Ins1*^{Cre};*Scn9a*$^{wt/wt}$ islets from both male and female mice. These effects of carbamazepine on insulin secretion *in vitro* were not additive to the effects of *Scn9a* knockout, suggesting that *Scn9a* is the main target of carbamazepine in β-cells that is relevant for insulin secretion. Complete *Scn9a* deletion also protected β-cells from death *in vitro*, similarly and non-additively to carbamazepine treatment. Finally, we assessed diabetes incidence in Nod.*Scn9a*$^{flox/flox}$ mice and NOD.*Ins1*^{Cre};*Scn9a*$^{wt/wt}$ mice injected with AAV8-*Ins1*^{Cre} virus and a found significant reduction in diabetes incidence in β-cell specific knockout mice compared with littermate controls. Collectively, our data show the *Scn9a* plays important roles in β-cell function, but also contributes to β-cell death and type 1 diabetes progression. *Scn9a* is a novel drug target to preserve β-cells in type 1 diabetes.

Introduction

In type 1 diabetes, insulin secreting pancreatic β-cells are mostly destroyed by autoimmune attack which leads to hyperglycemia and devastating disease complications[1]. Protecting β-cells from stress may therefore have therapeutic benefit[2], but there are few viable potential therapeutic approaches that directly promote β-cell survival. Excess electrical excitability, known as excitotoxicity, has been linked with increased cell death and dysfunction in multiple cell types, including pancreatic β-cells[3-5]. Insulin is a primary autoantigen both in murine and human type 1 diabetes pathogenesis[5,6]; β-cell hyper-activity may increase neo-autoantigens production, initiating and/or accelerating the disease[7]. Ion channels that mediate β-cell excitotoxicity are emerging as potential targets for type 1 diabetes prevention and delay. Most research so far has focused on targeting Ca^{2+} channels and ATP sensitive potassium channels[8,9]. The concept that excitotoxicity is a viable therapeutic target for early intervention in type 1 diabetes has been demonstrated in pre-clinical and clinical research focusing on verapamil, a voltage-gated Ca^{2+} channel inhibitor. Verapamil prevents diabetes and improves endogenous insulin secretion over the

long-term in type 1 diabetes mouse models[9]. Clinical trials reported beneficial effects of verapamil on human β-cell function in the context of type 1 diabetes, although this diminishes over time[10-12]. These studies emphasize the need to identify more drugs that can protect β-cells from excitotoxicity to prevent or treat type 1 diabetes.

Voltage-gated Na^+ channels have not been studied to the same extent as Ca^{2+} channels, and their physiological roles in β-cells remain controversial. Prominent Na^+ currents have been reported in human β-cells and other mammals[13-15]. In mouse β-cells, Na^+ channels have been reported to stay inactivated at resting membrane potentials and are therefore not believed to contribute to insulin secretion at physiological glucose concentrations[15-18]. The Na^+ channel blocker tetrodotoxin partially reduced glucose-induced insulin secretion in rat β-cells, especially at high glucose concentrations[19].

We previously showed that carbamazepine, a use-dependent Na^+ channel inhibitor used to treat epilepsy, protected β-cells[20] and significantly reduced diabetes incidence in NOD mice[21]. Of the genes encoding voltage-gated Na^+ channel α sub-units[22], *Scn9a* (Nav1.7) is the predominant isoform in mouse β-cells[23]. With the goal of studying the roles of *Scn9a* in normal β-cell function and death, and its contribution to type 1 diabetes initiation and the actions of carbamazepine, we used two new mouse models: 1) NOD mice with *Scn9a* floxed alleles ($Scn9a^{flox/flox}$) and a $Ins1^{Cre}$ knock-in allele ($Ins1^{Cre/WT}$) for lifelong deletion; 2) NOD mice with *Scn9a* floxed alleles injected with a pancreas-selective adeno-associated virus (serotype 8) carrying *Ins1* promoter driven Cre recombinase (AAV8-Ins1Cre) for a timed deletion of the *Scn9a* gene. We found that protective effects of carbamazepine in human islets were also shared with oxcarbazepine and spider toxin ProTxII. We observed that β-cell *Scn9a* is critical for the full activation of Na^+ currents and insulin release in response to high glucose, and that it mediates all of the effects of carbamazepine that we assessed. We also observed protection from type 1 diabetes in β-cell specific *Scn9a* knockout NOD mice. These data suggest that Na^+ channel-mediated excitotoxicity contributes significantly to type 1 diabetes pathophysiology.

Materials and Methods

Human Islets

Human islets from cadaveric donors were obtained from Alberta IsletCore program[25], with the written research consent of donors and their families and approval by the Human Research Ethics Board at the University of Alberta (Pro00013094). Human islet use was approved by the ethical board from the UBC Clinical Research Ethics Board (H13-01865). The following donor numbers where used: R317, R318, R322 and R395 for islet cell survival assay. R396, R398, R399, R406 and R407 for dynamic insulin secretion measured with islet perifusion *in vitro.* Full donor and isolation information can be found for these donors at www.isletcore.ca.

Genetic manipulation in mice

All animal procedures were in accordance with the Canadian Council for Animal Care guidelines. All animal studies and protocols were approved by the University of British Columbia Animal Care Committee. Mice were housed in the Centre for Disease Modelling specific pathogen-free facility on a standard 12-hour light/12-hour dark cycle with ad libitum access to chow diet (PicoLab, Mouse Diet 20-5058). To generate NOD:*Ins1*$^{cre/wt}$, we contracted Jackson Laboratories to backcross B6(Cg)-Ins1tm1.1(cre)Thor/J (Jackson Laboratory, No. 026801) > 12 times. NOD:*Scn9a*$^{flox/flox}$ mice were generated on the NOD/ShiLtJ background by the Jackson Laboratory. We backcrossed/refreshed each parent colony every 5th generation. Female *Ins1*$^{wt/wt}$;*Scn9a*$^{flox/wt}$ and male *Ins1*$^{cre/cre}$;*Scn9a*$^{flox/wt}$ mice were set up as breeders, at age 8 to 9 weeks, to generate experimental mice. Females from the parental colonies were included only once as breeders to eliminate the risk of onset of hyperglycemia during pregnancy and blood glucose measurements were done at time of weaning for each breeder female. Cohorts included in generation of Kaplan-Meier curves were monitored twice per week and was used only to determine hyperglycemia onset incidence and body mass changes. Diabetes was defined as 2 consecutive blood glucose measurements greater than or equal to 16 mmol/L or one measurement greater than or equal to 22 mmol/L and immediately euthanized. Cohorts generated for other *in vivo* and *in vitro* analyses were terminated at 12 (AAV8-*Ins1*-Cre) or 18 weeks (*Ins*1Cre) in a prediabetic phase. All animals were monitored for diabetes before used for analysis. For inducible knockout, VectorBuilder Inc. (Chicago, USA) generated AAV8-*Ins1*-Cre adeno-associated virus carrying *Ins1* promoter-driven Cre recombinase (AAV8-*Ins1*-Cre)[26]. All mice were injected into the intraperitoneal cavity with 1X10^{12} VGP of AAV8-*Ins1*-Cre virus at 6-7 weeks of age. Mice were examined 24-, 48-, and 72-hours following injection to ensure no infection or complications from procedure.

Islet isolations and dispersion

All mice for islet isolations were euthanized by CO_2, and immediately after, each pancreas was inflated through ductal injection then incubated with collagenase. This was followed by filtration and hand picking of islets as in our previous studies and following the same procedure as Luciani and Johnson[27]. Islets where either used whole or dispersed 24 hours post-isolation. For experiments with both human and mouse islets that required dispersions, islets were washed 4 times in (Ca^{2+}/Mg^{2+}-free Minimal Essential Medium for suspension cultures, Cellgro #15-015-CV). This was followed by gentle trypsinization (0.01%) by repeatedly pipetting up and down 30 times and resuspension in RPMI1640 (Thermo Fisher Scientific #11875-093), 10% FBS, 1% PS) and cultured as described[28].

Islet cell survival assay

Pancreatic islets from human cadaveric donors and NOD mice were dispersed according to the protocol above and subsequently seeded onto 384-well plates. Cells were stained with 50 ng/mL

Hoechst 33342 (Invitrogen) and 0.5 µg/mL propidium iodide (PI); we have shown that neither of these chemicals affect islet cell viability individually at these concentrations[20]. RPMI 1640 medium (Invitrogen) was supplemented to 5 mM glucose for human islets/cells and 10 mM glucose for mouse islets/cells. Media contained 100 U/mL penicillin, 100 µg/mL streptomycin (Invitrogen), 10% vol/vol FBS (Invitrogen). After 2 hours of staining, cells were incubated with a cytokine cocktail (25 ng/mL tumor necrosis factor-α (TNF-α), 10 ng/mL interleukin-1β (IL-1β), and 10 ng/mL interferon-γ (IFN-γ); R&D Systems) or thapsigargin (Millipore sigma). Immediately after the addition of test drugs (see table for overview), the cells were imaged at 37 °C and 5% CO_2. Images were captured every second hour for 72 hours using a robotic microscope (ImageXpress^{MICRO} XLS, Molecular Devices) and analyzed using the MetaXpress multi-wave cell scoring package (Molecular Devices).

Isoform expression of Sodium-channel α subunit

The Chan-Zuckerberg Biohub's CELLxGENE Discover Census with gget cellxgene module was used to query and analyze publicly available scRNA data (cellxgene.cziscience.com)[29]. Genes of interest were selected from the sodium voltage-gated channel α subunit gene group from the HGNC database (www.genenames.org). Human and mouse (mus musculus) scRNA data from pancreas were fetched from census version 2023-05-15. Dot plots of mean expression of each gene and fraction of expressed cells in each group were plotted with sc.pl.dotplot() function for both human and mouse results. Analysis was done in GoogleColab environment unless otherwise specified.

Electrophysiology

Islets shipped by overnight courier in RPMI 1640 medium from Vancouver to Edmonton. Islets were dispersed into single cells on the day of receipt and plated on 35-mm cell culture dishes as described previously[30]. Single cells were cultured in RPMI-1640 (11875, Gibco) with 11.1 mM glucose, 10 % FBS (12483, Gibco), 100 units/mL penicillin, and 100 mg/mL streptomycin (15140, Gibco) for 1-3 days. Cells were patch-clamped in the whole-cell or perforated voltage-clamp configuration in a heated bath at 32-35°C and patch pipettes with resistances of 4-5 MOhm after fire polishing. Whole-cell capacitance was recorded with the Sine+DC lock-in function of a HEKA EPC10 amplifier and PatchMaster software (HEKA Electronics, Germany) as previously described[30]. Exocytotic responses and Na^+ channel currents were measured 1-2 minutes after obtaining the whole-cell configuration. Exocytotic responses were measured in response to ten 500 ms depolarizations to 0 mV from a holding potential of -70 mV, and Na^+ channel currents were activated by the membrane potentials ranging from -120 to -20 mV. The bath solution contained (in mM): 118 NaCl, 20 tetraethylammonium-Cl, 5.6 KCl, 1.2 $MgCl_2$, 2.6 $CaCl_2$, 5 HEPES, and 5 glucose (pH 7.4 with NaOH). The patch pipettes were filled with (in mM): 125 Cs-glutamate, 10 CsCl, 10 NaCl, 1 $MgCl_2$, 0.05 EGTA, 5 HEPES, 0.1 cAMP and 3 MgATP (pH 7.15 with CsOH). Action potential measurements were performed in current-clamp mode of the perforated patch-

clamp configuration. The bath solution contained (in mM): 140 NaCl, 3.6 KCl, 1.5 $CaCl_2$, 0.5 $MgSO_4$, 10 HEPES, 0.5 NaH_2PO_4, 5 $NaHCO_3$, and indicated concentrations of glucose (pH 7.3 with NaOH). The patch pipettes were filled with (in mM): 76 K_2SO_4, 10 KCl, 10 NaCl, 1 $MgCl_2$ and 5 HEPES (pH 7.25 with KOH), and back-filled with 0.24 mg/ml amphotericin B (Sigma, cat# a9528). Mouse β- and α-cells were distinguished by characteristic differences in the voltage-dependent inactivation of Na^+ currents [31,32]. Data were analyzed using FitMaster (HEKA Electronics) and Prism (GraphPad Software Inc., San Diego, CA).

Dynamic Insulin Secretion

To measure the dynamics of insulin secretion, 65 human islets or 100 mouse islets were added to columns and perifused (0.4L/min) with 3 mM glucose KRB solution initially for 60 minutes, and then exposed to different concentrations of glucose as indicated in the figures and described previously[33]. Samples were stored at −20°C and insulin secretion was measured using a mouse insulin radioimmunoassay kit (Millipore Cat# HI-14K).

Calcium imaging

Islets where isolated and dispersed according to established protocol and seeded on poly-D-lysine-coated glass coverslips in a 200 µL media droplet for 5 hours followed by overnight incubation in 6 well cell culture plate with 2 mL media. Fura-2-AM (5 µM) was added 30 min prior to the start of the experiment. Coverslips were then washed in HEPES buffer (137 mM NaCl, 5.4 mM KCl, 0.25 mM Na_2HPO_4, 0.44 mM KH_2PO_4, 2 mM $CaCl_2$, 4.2 mM $NaHCO_3$, 3 mM glucose, 10 mM HEPES, pH 7.4) and placed in a chamber before imaging at 37°C on a Zeiss Axiovert 200M microscope with a 10x Alpha-PlanFluar (Zeiss, Germany), using a CoolSNAP HQ2 CCD camera (Photometrics, Tucson, USA). Fura-2 fluorescence ratio (F340/F380 excitation; emission 510 nm) was recorded every 10 seconds.

Histology, immunofluorescence and islet infiltration scoring

Pancreata were fixed in 4% paraformaldehyde for 24hours at 4°C and transferred to 70% ethanol for storage. Samples were paraffin embedded, sectioned, then stained with either hematoxylin/eosin (H&E), hematoxylin alone, terminal deoxynucleotidyl transferase dUTP nick end labelling (TUNEL), or insulin antibodies by WaxIT Histology Services Inc. (Vancouver, BC, Canada). Whole stained slides were imaged by WaxIT Histology Services at 20X magnification. 4 slices were made from 4 section 100µm apart to a total of 16 slides per animal excised and an additional slide from each section was processed unstained for subsequent immunohistochemistry experiments. H&E and TUNEL stained slides were scored blindly and mononuclear cell infiltrating islets cells were determined according to previous protocols[34]. Pancreatic β-cell area was quantified by normalizing insulin positive area to the respective section size as determined by DAPI staining and was reported as a ratio of the two numbers.

Additionally, insulin stain was used to determine insulitis proportion independent of H&E stain. To determine insulitis proportion, positive area was identified, and each islet was annotated, including mononuclear cells. Insulitis proportion was determined for each islet annotation analysis by normalizing non-insulin area to insulin positive area. The analysis from these annotations was subsequently used for quantification of strong positive insulin proportion and islet area. As described above, each islet was annotated (Insulin positive stain of the matching section was used to verify insulin positive area) for determination of TUNEL-positive proportion, with the exception that mononuclear cells were excluded. Images were analyzed using Aperio ImageScope software v12.4.0.5043 (Leica Biosystems, Wetzlar, Germany).

For *Scn9a* and β-cell proliferation immunofluorescence analyses, slides were de-waxed and rehydrated using 3 x 5 minutes of soaking in xylene and 5 minutes of soaking in 2 x 100% ethanol, 1 x 95% ethanol, and 1 x 75% ethanol. Slides were placed in 10 mM citrate buffer and subject to heat-induced epitope retrieval for 10 minutes at 95 ^{o}C. Slides were returned to room temperature and washed in deionized water followed by 1% PBS solution for 5 minutes each. Slides were removed from PBS solution and the circumference of pancreatic tissue was subscribed using ImmEdge Pen. Primary antibodies were diluted in DAKO Cytomation antibody diluent and 100-200 µL was added to each section of pancreatic tissue and incubated in a humid chamber overnight at 4C. The following day, slides were placed on a shaker at 80 RPM and rinsed with 1x PBS and washed for 3 x 10 minutes in 1xPBS. Secondary antibodies were diluted in DAKO Cytomation antibody diluent, then 100-200uL added to each section and incubated for 1 hour at room temperature. Secondary antibody solution was removed and slides were washed with PBS for 3x10 minutes. VECTASHIELD Hardset DAPI counterstain was applied to the tissue and sealed with a cover slip. Slides were left to set at room temperature overnight in a dry chamber. All steps in the protocol after introduction of secondary antibodies were conducted in the dark due to the light-sensitive nature of secondary antibodies.

For *Scn9a* immunofluorescence imaging, Raybiotech guinea pig anti-insulin antibody (cat# 129-10332) was used at 1:500 dilution and Invitrogen Scn9a rabbit polyclonal antibody (PA5-77727) at 1:250 dilution. JacksonImmuno secondary antibodies donkey anti-rabbit FITC (1:200) (cat#711-095-152) and donkey anti-guinea pig Cy3 (1:600) (cat#706-165-148) were used to counterstain. Slides were imaged on a Zeiss Axiovert 200M microscope with 20x air objective with standardized exposure times for each channel. Intensity thresholds were standardized in SlideBook software (Intelligent Imaging Innovations, Denver, USA). Images were exported as 8-bit TIFFs and merged using ImageJ.

For proliferation imaging, primary antibodies were Raybiotech guinea pig anti-insulin antibody (cat# 129-10332) at 1:500 dilution and New England Biolabs anti-rabbit proliferating cell nuclear antigen (PCNA) (D3H8P) XP® antibody at 1:800 dilution, and secondary antibodies were AlexaFluor anti-rabbit goat antibody and AlexaFluor anti-guinea pig antibody at 1:500 dilution. All images were taken on a Zeiss Axiovert 200M microscope with a 100x Alpha-PlanFluar NA 1.45 oil objective (Zeiss, Germany),

using a CoolSNAP HQ2 CCD camera (Photometrics, Tucson, USA). Number of proliferating β-cells was determined by PCNA positive nuclei completely insulin.

Metabolic physiology

For all physiological tests, littermates at 18 weeks of age were subjected to a 5-hour fast prior any test was carried out. Fasting bodyweight and basal blood glucose concentration were recorded. For intraperitoneal glucose tolerance tests (IPGTT) and in vivo insulin secretion tests, 20% glucose solution in saline was administered by intraperitoneal injection to each mouse based on body weight (2 g/kg). OneTouch glucose strips and a OneTouch Ultra2 glucose meter were used to measure glucose in blood drawn from the tail vein. Blood collections for in vivo insulin section and insulin tolerance test (ITT) was collected from the saphenous vein. To minimize stress, animals were shaved to expose the saphenous vein prior to the fast.

RNA sequencing and pathway analysis.

100 islets from each mouse where isolated according to method above and incubated for 24 hours and immediately flash-frozen in liquid nitrogen and stored at −80 °C. RNA was isolated using RNeasy Mini Kit (Qiagen #74106) according to manufacturer's instructions. 60 million read depth were performed and library preparation, RNA sequencing, and bioinformatics support were provided by the UBC Biomedical Research Centre Core Facility (Vancouver, BC, CA). Sample quality control was performed using the Agilent 2100 Bioanalyzer System (RNA Pico LabChip Kit). Sequencing was performed on the Illumina NextSeq 500 with paired end 42bp × 42bp reads. Demultiplexed read sequences were then aligned to the reference sequence (UCSC mm10) using STAR aligner (v 2.5.0b)[35]. Differential expression analysis was analyzed using DESeq2 R package[36]. Pathway enrichment was performed using the clusterProfiler R package with the Gene Ontology Molecular Function database[37].

Statistics and data analysis.

Data are expressed as mean ± standard error of the mean (SEM). Statistical analysis was performed using the Mann-Whitney test, one-way ANOVA, or repeated measures two-way ANOVA as indicated. Diabetes incidence was measured by Kaplan-Meier analysis and quantified by log-rank test. (GraphPad Prism, GraphPad Software Inc., La Jolla, USA). Unless otherwise stated, *p* values <0.05 were considered significant.

Results

Effects of Na^+ channel modulators on cell death and insulin secretion in human islets.

We have previously shown that carbamazepine improves survival in MIN6 cells and primary mouse islet β-cells, both *in vitro* and *in vivo*[21,38]. As a next step towards clinical translation, we tested whether

the pro-survival effects of carbamazepine were translatable to human β-cells and generalizable to other Na^+ channel inhibitors. We used our high-throughput, multi-parameter, kinetic imaging platform[20] and dispersed human islet cells to compare the effects of Na^+ channel modulator drugs on survival in the presence a cytotoxic cytokine cocktail containing TNF-α, IL-1β, and IFN-γ, or a DMSO/vehicle control. We also tested the effects of each drug on ER stress-associated β-cell death induced by the ER Ca^{2+} pump inhibitor thapsigargin[39]. Carbamazepine protected human islet cells from both cytokine-induced and ER-stress-induced apoptosis in a dose-dependent manner (Fig. 1A). Oxcarbazepine, a structurally related analog of carbamazepine, demonstrated similar dose-dependent pro-survival effect on human islet cells in the presence of both thapsigargin and cytokines (Fig. 1B). Interestingly, spider toxin ProTxII and ambroxol were only protective in the context of thapsigargin (Fig. 1C,D). Veratridine, an enhancer of voltage-dependent Na^+ channels, exhibited the opposing effect, by increasing cell death (Fig. 1E). Collectively, our data demonstrates that the pro-survival properties of carbamazepine in human islet cells mirrors previous findings in MIN6 cells and mouse primary β-cells[20]. Inhibition of voltage-gated Na^+ channels may improve the survival rate of β-cells through suppression of excitotoxicity.

We next examined the effects of Na^+ channel-modulating drugs on glucose-stimulated insulin secretion from intact human islets. Addition of 20 μM carbamazepine reduced insulin secretion at 15 mM glucose or 30 mM KCl (Fig. 2A). Oxcarbazepine, spider toxin ProTxII, and ambroxol did not significantly reduce insulin secretion under these conditions (Fig. 2B-D). Veratridine potentiated insulin secretion at 15 mM glucose (Fig. 2 D). Together, these experiments show that, in general, protective Na^+ channel modulating drugs tend to have modest effects on insulin secretion (Fig. 2F).

Expression of Na^+ channel subunits in human and mouse islet cells

Multiple genes encode voltage-gated Na^+ channels[22]. Multiple studies have reported that the Na^+ channel isoform with the highest expression level in β-cells is encoded by the gene *Scn9a* (Nav1.7)[20,24,40]. *Scn9a* was reported to account for approximately 80% of total Na^+ channel mRNA expression in whole mouse islets[41]. We investigated the cell type-specific expression of Na^+ alpha subunit genes using a publicly available single cell RNA sequencing dataset compiled from multiple studies, in humans and mice. *SNC9A*/*Scn9a* was found in all islet cell types and was the most frequently expressed of the Na^+ genes in single pancreatic β-cells, from human or mouse islets (Fig. 3A,B). These data demonstrate the islet cell type specific nature of Na^+ alpha subunit gene expression and the need to study *Scn9a* with a β-cell specific genetic manipulation.

A cell-specific Scn9a knockout NOD mouse model with reduced β-cell Na^+ current.

To study the effect of β-cell specific deletion of *Scn9a* in NOD mice, we generated $Scn9a^{flox/flox}$;$Ins1^{Cre/wt}$ ($Scn9a^{KO}$), $Scn9a^{wt/flox}$;$Ins1^{Cre/wt}$ ($Scn9a^{HET}$) and $Scn9a^{wt/wt}$;$Ins1^{Cre/WT}$ ($Scn9a^{WT}$)

littermates (Fig. 4A). Immunofluorescence imaging with a *Scn9a* antibody illustrated an expected reduction in fluorescence intensity in *Scn9a*- deficient β-cells (Fig. 4B). Criticaly, *Scn9a*^{KO} β-cells had almost entirely abolished Na^+ current compared *Scn9a*^{WT} (Fig. 4C,D), while β-cells from *Scn9a*^{HET} mice had intermediately reduced Na+ currents. These measurements verify functional loss of *Scn9a* action in our model and show that *Scn9a* is the major functional isoform in β-cells.

Full *Scn9a* deletion did not change voltage-dependent Ca^{2+} currents (Fig. 4E,F). In perforated patch configuration current-clamp, the oscillatory pattern from *Scn9a*^{KO} β-cells were easily distinguished from those seen in *Scn9a*^{WT} control mice (Fig. 4G). Interestingly, action potential firing rate in *Scn9a*^{KO} β-cells was significantly increased at 6 mM and 12 mM glucose (Fig. 4G,H). Firing thresholds was significantly reduced in *Scn9a*-deficient β-cells (Fig. 4I), however there was no difference in action potential height (Fig. 4J). It has been suggested that Na^+ channels contribute to Ca^{2+} current-induced action potentials in β-cells leading to increased insulin secretion in response to glucose[40]. Collectively, these data suggest that *Scn9a* Na^+ channels play an important role of β-cell electrical activity.

Scn9a is required for high glucose response and mediates the effects of carbamazepine.

Expression of multiple isoforms of Na^+ channels has been reported in mouse β-cells[20,40], we were therefore interested in the proportion of glucose-stimulated insulin secretion that is contributed by *Scn9a* channels. We assessed insulin secretion in response to a step-ramp of increasing glucose from islets isolated from both male and female NOD mice, that were not diabetic (see below; Fig. 5.A and B). We found a reduction in insulin secretion from both male and female *Scn9a*^{KO} mice when compared to wildtype littermate controls, which was significant at 15 mM glucose, but not at more moderate glucose challenges (Fig. 5A,B). This agrees with previously published static incubation studies showing that insulin secretion response to 10 mM glucose was not different in *Scn9a* deficient β-cells, at least when compared with *Scn9a* heterozygous cells[24]. Carbamazepine significantly reduced insulin secretion from male and female *Scn9a*^{WT} mice (Fig. 5A,B). Importantly, the drug-induced reduction at 15 mM glucose-stimulated insulin secretion was absent in *Scn9a*^{KO} mice, demonstrating that carbamazepine's effect on insulin secretion is mediated through the *Scn9a* channel.

Insulin secretion is dependent on intracellular Ca^{2+} signalling. To further define the molecular mechanisms of defective insulin secretion at 15 mM glucose in *Scn9a* deficient β-cells, we loaded dispersed β-cells with Fura-2 to measure cytoplasmic Ca^{2+}, which includes the contribution of multiple Ca^{2+} sources. In *Scn9a*^{KO} β-cells, Ca^{2+} levels appeared elevated at baseline in 3 mM glucose (Fig. 5C). When normalized to baseline, we found a significant decrease in Ca^{2+} influx at 15 mM glucose exposure (Fig. 5C, *inset*), consistent with the dynamic insulin secretion data above. Voltage-dependent increases in plasma membrane capacitance in patch-clamped β-cells, which reflect the distal steps in exocytosis, were not different between *Scn9a*^{KO} mice and controls (Fig. 5D). These findings indicate that the

selective reduction in 15 mM glucose-stimulated insulin secretion is associated with reduced Ca^{2+} responsive from baseline, rather than a block of distal exocytotic machinery.

Scn9a is required for stress-induced β-cell death and mediates the effects of carbamazepine.

We have established that pharmacological inhibition of Na^+ channels protects MIN6 cells[20], primary mouse islets, and human islets (Fig. 1) from stresses relevant to type 1 diabetes. To test the hypothesis that β-cell specific removal of the *Scn9a* channel protects primary murine β-cells from cytokine-induced and thapsigargin-induced apoptosis, we employed the same multi-parameter imaging platform used to measure cell death in human islet cells above and dispersed cells from our *Scn9a*-deficient model. Cytokines and thapsigargin reproducibly induced death in primary islet cells from wildtype mice, whereas cells lacking *Scn9a* were almost completely protected (Fig. 6A). We used cells from controls and β-cell specific *Scn9a* knockouts to determine the contribution of this gene product to the pro-survival effects of carbamazepine[20]. As expected, carbamazepine reduced cell death levels to those observed in DMSO controls, in *Scn9a*^{WT} islet cell exposed to cytokines and thapsigargin (Fig. 6A). However, addition of carbamazepine to *Scn9*a-deficient β-cells did not yield a further reduction in cell death, suggesting that the pro-survival effects of carbamazepine are primarily mediated through the *Scn9a* channel. These data again point to the striking specificity of carbamazepine for β-cell *Scn9a* and rule out major off-target effects.

Diabetes incidence and glucose tolerance in β-cells lacking Scn9a and one allele of Ins1.

Our β-cell specific *Scn9a* knockout mice were generated using the *Ins1*^{Cre} knock-in/replacement allele, which we have recently reported significantly delays and protects from type 1 diabetes on its own due to both the loss of the autoantigenic *Ins1* allele and presence of Cre itself[42]. Consistent with this, we observed no significant difference in diabetes incidence after 50 weeks of monitoring female NOD.*Scn9a*^{flox}-*Ins1Cre* mice and no male mice of either genotype developed diabetes (Fig. 7AB). Traditional blinded, manual, and categorical insulitis scoring was unable to identify significant differences between genotypes in male or female mice (Fig. 7C). We developed a new pipeline for this study, which instead of relying on semi-subjective categorization[34], uses an objective computer-based continuous quantification of the ratio of insulin positive staining-to-insulitis. We found a modest decrease in insulitis scores in male *Scn9a*^{KO} mice when compared to wildtype littermate controls, in both sexes (Fig. 7D,E), despite the absence of a detectable difference in diabetes incidence (Fig. 7B). This observation suggests that *Scn9a* may alter immune cell attraction to islets or infiltration into islets.

A positive outcome of this allele configuration was that we could determine physiological and cellular phenotype of these mice prior to diabetes (see above). To further investigate the phenotype associated with *Scn9a* loss of function in NOD mice, we conducted *in vivo* studies on 18 week old male and female mice. *In vivo* insulin secretion 15 minutes after glucose challenge was significantly reduced in *Scn9a*^{KO}

male and female mice relative to *Scn9a*^{WT} littermate controls (Fig. 7F,H). Glucose tolerance was unaffected (Fig. 7G,I), indicating that, while lower than controls, *Scn9a*^{KO} mice have sufficient insulin capacity to maintain glucose homeostasis.

To determine the roles of *Scn9a* on β-cell turn-over *in vivo*, and without the confounder of diabetes, we stained pancreas sections from 18-week-old NOD mice for insulin and TUNEL. Apoptosis at this age was unaffected by β-cell specific *Scn9a* deletion (Fig. 7J,K). We also found no difference in proliferating cell nuclear antigen (PCNA)-positive β-cells at this time-point (Fig. 7L,M). Using the new pipeline and annotation tool mentioned above, we found no significant differences in insulin staining intensity (Fig. 7N,O) or islet size (Fig. 6P). Notwithstanding, we did observe a modest, but statistically significant reduction in β-cell area in male and female *Scn9a* KO mice relative to controls (Fig. 7Q), perhaps resulting from earlier differences in β-cell turnover. We next examined islet insulin content because we have previously reported that carbamazepine increases insulin production[38] and isolated islets from global *Scn9a* knockout mice accumulate insulin protein in their β-cells[38]. We observed no significant increase in insulin content from isolated islets in our specific β-cell *Scn9a* KO mouse model (Fig. 7R). Collectively, these data point to a minor role for *Scn9a* in the maintenance of normal β-cell mass under normal non-diabetic conditions.

AAV8-Ins1Cre mediated deletion of Scn9a reduces diabetes incidence in NOD mice.

To overcome the limitation associated with replacing a single *Ins1* gene with Cre recombinase in our NOD.*Ins1*^{Cre};*Scn9a*^{flox} mice[42], we instead used the pancreas-biased AAV8 virus serotype and a highly specific *Ins1*-promoter to deliver Cre specifically to β-cells for deletion of *Scn9a* at 6-7 weeks (Fig. 8A). This approach has been reported to have comparable efficiency to Cre driver line models[26]. First, we demonstrated high recombination efficiency and specificity with AAV8 *Ins1*-GFP in islets from NOD WT (Fig. 8B). Based on previous studies showing that carbamazepine reduces diabetes incidence in NOD mice[21] and surmising that this effect is primarily mediated through the *Scn9a* channel, we hypothesized that β-cell specific removal of *Scn9a* in NOD would exhibit a similar delay in diabetes. Indeed, we observed a significant reduction in diabetes incidence between *Scn9a*^{KO} and *Scn9a*^{WT} female mice (Fig. 8C). Somewhat paradoxically, this protection was despite a significant reduction in glucose-stimulated insulin secretion *in vivo* (Fig. 8D). Also mirroring what we observed in non-diabetic conditions above, there was no significant difference in glucose tolerance (Fig. 8E). We did not observe any difference between insulitis proportions, insulin positive area, or strong insulin positive cell proportion (Fig. 8. F-H). Collectively, our data demonstrated that β-cell *Scn9a* deletion at 6-7 weeks using AAV8-*Ins1*Cre can prevent 50% of diabetes cases in our NOD mouse population by 30 weeks of age.

Transcriptomic analysis of β-cell specific Scn9a knockout islets

To identify the molecular mechanisms mediating the effects of *Scn9a* deletion, we performed RNA sequencing on isolated islets (Fig. 9). First, we confirmed that *Scn9a* mRNA (exon 3) was significantly reduced in whole islets from *Scn9a*^{KO} mice (3.5-fold decrease in islets that also contain non-β-cells; Fig. 9A). There were 5 other significantly decreased mRNAs in *Scn9a*^{KO} islets (Fig. 9B,C). Neuropeptide Y (*Npy*) has been implicated in β-cell function and survival[43,44]. Cytochrome P450-26B1 (*Cyp26b1*) is involved in embryonic development and cell differentiation[45]. Interestingly, Cyp26b1 degrades carbamazepine[46] and carbamazepine has a negative effect on cytochrome P450 enzyme activity and expression[47]. The farnesoid X receptor (*Nr1h4*) has multiple roles in β-cells[48]. Seven in absentia homolog 2 (*Siah2*) is responsible for degradation of proteins and involved in cellular processes including cell cycle progression, DNA repair, apoptosis, and hypoxia response[49].

We identified 13 mRNAs that were significantly increased in *Scn9a*^{KO} islets. Strikingly, we found multiple genes associated the major histocompatibility complex (MHC) class I and II were upregulated in islet cells from *Scn9a*-deficient mice (Fig. 9B,C), including H2-BI, H2-Q2, and H2-DMB1 (also known as H2-M; class II), which are involved in antigen presentation to CD8-positive T cells[50-52]. There was an increase in the CD8 alpha subunit mRNA in these islets. Both the H2-Q2 and H2-DMB1 genes have been implicated in the development of autoimmunity in NOD mice[53,54] In accordance, we found the 3 top pathways enriched in this analysis, MHC protein complex binding, peptide antigen binding, and antigen binding, are all involved in the process of presenting antigens to the immune system[55](Fig. 9D). Solute carrier family 2 member 6 (*Slc2a6*; aka GLUT6) was upregulated in *Scn9a*^{KO} islets. Interestingly, pancreatic islets isolated from GLUT6-deficient *Lep*$^{ob/ob}$ mice secreted a greater amount of insulin in response to high levels of glucose compared to wildtype controls[56]. Other upregulated genes included: pleckstrin homology domain containing A2 (*Plekha2*), which binds specifically to phosphatidylinositol 3,4-diphosphate and localize proteins to the membrane; proteasome 20S subunit beta 9 (*Psmb9*), a component of the proteosome; N-acetyl-alpha-glucosaminidase (*Naglu*), which degrades heparan sulfate; guanylate binding protein family member 6 (Gbp6/8/11), which is involved in cytokine signalling and confers protection from pathogens; NRAS proto-oncogene GTPase (*Nras*); angiopoietin 4 (*Angpt4*), which regulates the receptor tyrosine kinase TEK/TIE2. These observations, on balance, suggest that the *Scn9a* channel in β-cells could directly or indirectly modulate the immune system and provides further insight into the molecular mechanism of β-cell protection in type 1 diabetes.

Effects of heterozygous deletion of β-cell Scn9a

Isolated β-cells from *Scn9a*^{HET} mice had intermediately reduced Na^+ currents, as noted above (Fig. 3C,D). Perforated patch configuration voltage-clamp showed that the oscillatory pattern from heterozygous *Scn9a*- deficient β-cells were distinguishable from those seen in *Scn9a*^{WT} control mice (Fig. S1A), at 6 mM and 12 mM glucose, firing action potential, firing thresholds and potential height were unchanged (Fig. S1B). Collectively, these data suggest that heterozygous deletion of β-cell *Scn9a*

is associated with a small change oscillatory pattern but not enough to cause significant changes in β-cell electrical activity. Cytosolic Ca^{2+} levels appeared elevated at baseline in 3 mM glucose in β-cells from *Scn9a*^{HET} mice. When normalized to baseline, we found a significant decrease in calcium influx at 15 mM glucose exposure in Scn9a^{HET} β-cells (Fig. S1C), similar to *Scn9a*^{KO} β-cells (Fig. 4C). Despite this, insulin secretion from *Scn9a*^{HET} β-cells was more inhibited *Scn9a*^{KO} β-cells, with a near complete block of insulin secretion at all glucose concentrations (Fig. S1D,E). This was associated with an apparent inhibition of distal exocytosis mechanisms (Fig. S1F). In contrast to *Scn9a*^{KO} mice, *Scn9a*^{HET} mice demonstrated significantly worse glucose tolerance than their *Scn9a*^{WT} littermates, likely as a result of a more severe *in vivo* defect in glucose-stimulated insulin secretion (Fig. S2A-C). This indicates that *Scn9a*^{HET} mice have insufficient insulin capacity to maintain glucose homeostasis. Type 1 diabetes incidence was higher and more rapid onset in life-long *Scn9a*^{HET} females and unchanged in males (Fig. S2D,I). AAV8-*Ins1*Cre mediated removal of *Scn9a* at 6-7 weeks also resulted in an apparent acceleration of type 1 diabetes in female NOD mice (Fig. S3A), associated with reduced insulin response to glucose (Fig. S3B) and impaired glucose tolerance (Fig. S3C). *Scn9a*^{HET} mice from the AAV8-*Ins1*Cre cohort exhibited increased insulitis (Fig. S3D). Mechanistically, *Scn9a*^{HET} primary islet cells showed little to no protection from cytokine- or thapsigargin-induced death *in vitro* (Fig. S4A). In fact, we observed a significant increase in TUNEL positive cells, as well as a concomitant reduction in insulin area and insulin-positive cell number (Supplementary Fig. 4B-D). Interestingly, islet insulin content was increased in islets isolated from *Scn9a*^{HET} mice relative to controls (Fig. S4E). Together, these data point to a complex effect of partial *Scn9a* loss in β-cells.

Discussion

The goal of the present study was to investigate the roles of Na^+ channels in β-cells and drugs that can modulate them. We found that multiple Na^+ channel-modulators can protect human islet cells from stresses associated with type 1 diabetes while moderately decreasing insulin secretion in response to high glucose. Further, we show that β-cell specific, complete deletion of the major isoform, *Scn9a*, mimics and mediates these effects, and can protect mice from type 1 diabetes if induced after weaning. Our findings add support to the concept that a form of excitotoxicity plays a critical role in type 1 diabetes and suggest that use-dependent Na^+ channels inhibitors could be viable as future therapeutics to intervene in type 1 diabetes.

The roles of ion channels in β-cells have been extensively studied in rodents, however there may be important differences in channels expression and properties between rodent and human β-cells[57]. These differences can have significant effects on β-cell electrical activity and insulin secretion, highlighting the need for further investigation of human β-cell ion channels and their regulation in health and disease. In the current study, we found that carbamazepine protected human islet cells in a dose-dependent

manner from both cytokine- and ER stress-mediated cell death, while having modest inhibitory effects in insulin secretion. These findings confirm that carbamazepine's previously demonstrated protection from cell death of MIN6[38] cells and mouse β-cells[20] can be translated to human β-cells. Despite previous reports that carbamazepine may act via modulation of K_{ATP} channel trafficking[58], structurally related and unrelated Na^+ channel inhibitors had similar effects and the enhancement of Na^+ channel activity by veratridine had converse effect on both cell survival and glucose-stimulated insulin secretion. Thus, the effects of carbamazepine in human β-cells are likely specific to Na^+ channels.

Our work provides evidence to support the concept that suppression of excitotoxity is a key mechanistic target for type 1 diabetes prevention and therapeutic intervention. Consistent with the ability of Na^+ channel inhibition to protect neurons[59], previous findings from our lab suggested that reducing voltage-gated Na^+ channel activity with carbamazepine protects β-cells from apoptosis[20]. We found in the current study that oxcarbazepine also reduced cell death, however without reducing glucose-stimulated insulin secretion. We found that other Na^+ channel inhibitors, spider toxin ProTxII and ambroxol, were only protective in the context of ER stress-mediated cell death and did not significantly affect glucose-stimulated insulin secretion in human islets. These differences could be explained by Na^+ channel selectivity, as spider toxin ProTxII is more selective for *Scn9a*[60] while ambroxol is more selective for *Scn10a*[61], while carbamazepine has been shown to selectively target *Scn3a* and *Scn9a*[62]. Thus, the beneficial effects of carbamazepine could be mimicked by its analogues or other structurally unrelated drugs, without significant effects on insulin secretion.

Our study adds to our knowledge of the physiological and pathophysiological roles of Na^+ channels in β-cells. It was previously believed that Na^+ channels are more active in human, canine, and porcine β-cells than in rodent cells[15]. However, our findings reinforce that Na^+ channels in mouse β-cells should not be disregarded. Other studies have demonstrated that Na^+ currents are present in mice[63] and in β-cell lines[41]. Conditional *Scn9a* deletion in β-cells using an *Ins2* promoter-driven Cre transgenic mouse found reduced Na^+ current density and a non-significant trend towards decreased insulin secretion at 10 mM glucose[24]. However, these studies have the caveat that heterozygous controls were used rather than wildtype controls with the normal complement of *Scn9a* channel[24]. Here, we show that the *Scn9a* channel plays an active role in insulin secretion in response to 15 mM glucose, which is probably above the normal physiological range (but may be in a pathophysiological range). It has previously been shown that the inhibitor effect of TTX on insulin secretion also appears to increase with an increasing glucose concentration[64]. Our results suggest that *Scn9a*'s effect on insulin secretion at high glucose levels might be coupled to Ca^{2+}-handling as we observed changes in intracellular Ca^{2+} at similar high glucose concentrations in *Scn9a*-deficient β-cells. Interestingly, prolonged exposure to high glucose levels can lead to reduced insulin secretion and eventual dysfunction of pancreatic β-cells[65], known as

glucotoxicity[66].Glucotoxicity can result in hyperexcitability of β-cells, a process that may be linked to type 1 diabetes pathogenesis[67].

Excitotoxicity is a term often used to describe the sustained rise of intracellular Ca^{2+} in excitable cells[68]. It has been suggested that excitotoxicity may be a contributing factor to pancreatic β-cell failure, in both type 1 diabetes and type 2 diabetes[69,70]. Interestingly, we observed an increase in action potential frequency and a decrease in AP firing threshold in *Scn9a*^{KO} β-cells, indicating that these cells have increased excitability by some definititions[72]. Elevation in the intracellular Ca^{2+} concentration has been found in rat islets, exposed to prolonged high glucose[71], and mice with dysfunctional K_{ATP} channels exhibiting chronic, continuous action potential firing[5]. This suggests that an excess in electrical excitability and hyperactivity is a fundamental determinant of stress-induced β-cell failure. We found in this study that the *Scn9a*-deficient β-cells from NOD mice were protected from ER-stress and cytokines induced death. Of note, we did not see a further improvement in islet cell survival from *Scn9a*^{KO} mice when carbamazepine was added. These findings demonstrate that the pro-survival effect of carbamazepine is primarily mediated through the *Scn9a* channel. Similarly, the addition of carbamazepine to *Scn9a*-deficient β-cells did not further reduce insulin response to glucose. These findings seem to suggest that reduced excitability and the subsequent reduction in insulin secretion viably protects β-cells from metabolic stress and excitotoxicity.

We found that *Scn9a*^{HET} mice displayed a similar phenotypic effect on reduced insulin response to glucose, however, they exhibited an exaggerated phenotype that was not associated with the same protective effect observed in the *Scn9a*^{KO} mice. The exaggerated phenotype was associated with an increase in insulitis, islet apoptosis, as well as a concomitant reduction in insulin area. It is interesting to note that in wildtype NOD mice, a 70% reduction in β-cell mass has been observed after the onset of diabetes. Furthermore, insulin secretion was reduced to a greater extent than β-cell mass in these mice[75]. This phenomenon was hypothesized to be caused by the toxic effects of elevated glucose levels on β-cell function. Thus, it is possible that *Scn9a*^{HET} phenotype, is a product of inappropriate glucose handling, explained by a reduction in the distal exocytotic machinery leading to reduced β-cell function through the toxic effect of elevated glucose levels. This hypothesis is supported by the finding that *Scn9a*^{HET} mice demonstrated a decrease in glucose tolerance. Indeed, these differences could be explained by a compensatory pathway activated in *Scn9a*^{KO} mice which remains inactivated in *Scn9a*^{HET} mice. This idea is supported by the findings that RNA sequencing of primary islet cells from Scn9a^{KO} mice showed a range of significant differences in gene expression, while this was not observed in *Scn9a*^{HET} mice. It is also important to note that the exaggerated phenotypes associated with *Scn9a*^{HET} mice observed in our study suggest that from previous studies may need to be re-evaluated. Past work has assigned a relatively minor functional role to *Scn9a* in β-cells[24], however those studies used *Scn9a* heterozygous mice as controls, and our results suggest that this control might be inappropriate. A major finding of our study was that post-weaning β-cell specific *Scn9a* deletion using AAV8-*Ins1*Cre, was

associated with protection from type 1 diabetes. These results differ from the observations made in our *Ins1*^{Cre} mice. These inconsistencies are believed to be mainly attributed to the removal of a single Ins1 allele and the associated changes in insulin dosage[42,76] While the AAV8-*Ins1*Cre mouse model addresses the limitations associated with insulin dosage, it still relies on Cre to create gene conditional knockouts and as a result is restricted by the protective effects of Cre expression in NOD, beyond losing one Ins1 allele[42]. However, we observed that diabetes incidence rates in our WT AAV8-*Ins1*Cre control were comparable to wildtype controls with no AAV8-*Ins1*Cre and previously reported in WT NOD mice[77,78], regardless of housing facility differences. This suggests that the delivery of Cre via AAV8 virus at the 6–7-week time point does not confer protection against diabetes. There are two likely explanations for the discrepancy in Cre's protectiveness: 1) the method of introduction, whether by package recombinant AAV for gene delivery or Cre itself being inserted into the genome, or 2) the timing of which Cre is introduced. It has previously been reported that the timing of which coxsackievirus is introduced to NOD mice yields the opposing effects on diabetes development[79], by prevention at early exposure and accelerating at late. These findings seem to suggest that timing could be crucial, and that exposing mice to Cre recombinase in early stage or during development is causing the delay in diabetes development. Additionally, our findings that *Scn9a* is involved in diabetes development in NOD mice has been suggested in other studies, where carbamazepine treated animals demonstrated similar protection[21]. Our findings suggest that key cellular target of this anticonvulsant medication and its main mediator on pancreatic β-cell is the *Scn9a* channel.

It will be important to verify clinically that carbamazepine does not have deleterious effects on glucose homeostasis in the context of type 1 diabetes. Carbamazepine administration in people living with epilepsy has not been reported to affect blood glucose levels[74]. We found that *Scn9a*-deficient NOD mice did not demonstrate dysfunctional glucose tolerance. Although, these findings suggest that there may be a low risk associated with administration of carbamazepine to patients in a prediabetic phase, careful consideration should be made to evaluate the potential impact of reduced insulin secretion under glycemic condition in the context of carbamazepine treatment.

In summary, our observations suggest that Na^+ channels are a promising candidate for future development of therapeutics that aim to protect β-cells. A repurposed drug like carbamazepine that can enhance β-cell survival in type 1 diabetes may have a shortened path to the clinic.

References

1 Dotta, F. & Eisenbarth, G. S. Type I diabetes mellitus: a predictable autoimmune disease with interindividual variation in the rate of beta cell destruction. *Clin Immunol Immunopathol* **50**, S85-95, doi:10.1016/0090-1229(89)90115-3 (1989).

2 Page, K. A. & Reisman, T. Interventions to preserve beta-cell function in the management and prevention of type 2 diabetes. *Curr Diab Rep* **13**, 252-260, doi:10.1007/s11892-013-0363-2 (2013).

3 Osipovich, A. B., Stancill, J. S., Cartailler, J. P., Dudek, K. D. & Magnuson, M. A. Excitotoxicity and Overnutrition Additively Impair Metabolic Function and Identity of Pancreatic beta-Cells. *Diabetes* **69**, 1476-1491, doi:10.2337/db19-1145 (2020).

4 Speckmann, T., Sabatini, P. V., Nian, C., Smith, R. G. & Lynn, F. C. Npas4 Transcription Factor Expression Is Regulated by Calcium Signaling Pathways and Prevents Tacrolimus-induced Cytotoxicity in Pancreatic Beta Cells. *J Biol Chem* **291**, 2682-2695, doi:10.1074/jbc.M115.704098 (2016).

5 Stancill, J. S. *et al.* Chronic beta-Cell Depolarization Impairs beta-Cell Identity by Disrupting a Network of Ca(2+)-Regulated Genes. *Diabetes* **66**, 2175-2187, doi:10.2337/db16-1355 (2017).

6 Choo, S. Y. The HLA system: genetics, immunology, clinical testing, and clinical implications. *Yonsei Med J* **48**, 11-23, doi:10.3349/ymj.2007.48.1.11 (2007).

7 Rodriguez-Calvo, T., Johnson, J. D., Overbergh, L. & Dunne, J. L. Neoepitopes in Type 1 Diabetes: Etiological Insights, Biomarkers and Therapeutic Targets. *Front Immunol* **12**, 667989, doi:10.3389/fimmu.2021.667989 (2021).

8 Drews, G., Krippeit-Drews, P. & Dufer, M. Electrophysiology of islet cells. *Adv Exp Med Biol* **654**, 115-163, doi:10.1007/978-90-481-3271-3_7 (2010).

9 Xu, G., Chen, J., Jing, G. & Shalev, A. Preventing beta-cell loss and diabetes with calcium channel blockers. *Diabetes* **61**, 848-856, doi:10.2337/db11-0955 (2012).

10 Forlenza, G. P. *et al.* Effect of Verapamil on Pancreatic Beta Cell Function in Newly Diagnosed Pediatric Type 1 Diabetes: A Randomized Clinical Trial. *JAMA* **329**, 990-999, doi:10.1001/jama.2023.2064 (2023).

11 Xu, G. *et al.* Exploratory study reveals far reaching systemic and cellular effects of verapamil treatment in subjects with type 1 diabetes. *Nat Commun* **13**, 1159, doi:10.1038/s41467-022-28826-3 (2022).

12 Ovalle, F. *et al.* Verapamil and beta cell function in adults with recent-onset type 1 diabetes. *Nat Med* **24**, 1108-1112, doi:10.1038/s41591-018-0089-4 (2018).

13 Silva, A. M., Dickey, A. S., Barnett, D. W. & Misler, S. Ion channels underlying stimulus-exocytosis coupling and its cell-to-cell heterogeneity in beta-cells of transplantable porcine islets of Langerhans. *Channels (Austin)* **3**, 91-100, doi:10.4161/chan.3.2.7865 (2009).

14 Barnett, D. W., Pressel, D. M. & Misler, S. Voltage-dependent Na+ and Ca2+ currents in human pancreatic islet beta-cells: evidence for roles in the generation of action potentials and insulin secretion. *Pflugers Arch* **431**, 272-282, doi:10.1007/BF00410201 (1995).

15 Pressel, D. M. & Misler, S. Sodium channels contribute to action potential generation in canine and human pancreatic islet B cells. *J Membr Biol* **116**, 273-280, doi:10.1007/BF01868466 (1990).

16 Gopel, S. *et al.* Capacitance measurements of exocytosis in mouse pancreatic alpha-, beta- and delta-cells within intact islets of Langerhans. *J Physiol* **556**, 711-726, doi:10.1113/jphysiol.2003.059675 (2004).

17 Plant, T. D. Na+ currents in cultured mouse pancreatic B-cells. *Pflugers Arch* **411**, 429-435, doi:10.1007/BF00587723 (1988).

18 Gopel, S., Kanno, T., Barg, S., Galvanovskis, J. & Rorsman, P. Voltage-gated and resting membrane currents recorded from B-cells in intact mouse pancreatic islets. *J Physiol* **521 Pt 3**, 717-728, doi:10.1111/j.1469-7793.1999.00717.x (1999).

19 Hiriart, M. & Matteson, D. R. Na channels and two types of Ca channels in rat pancreatic B cells identified with the reverse hemolytic plaque assay. *J Gen Physiol* **91**, 617-639, doi:10.1085/jgp.91.5.617 (1988).

20 Yang, Y. H., Vilin, Y. Y., Roberge, M., Kurata, H. T. & Johnson, J. D. Multiparameter screening reveals a role for Na+ channels in cytokine-induced beta-cell death. *Mol Endocrinol* **28**, 406-417, doi:10.1210/me.2013-1257 (2014).

21 Lee, J. T. C., Shanina, I., Chu, Y. N., Horwitz, M. S. & Johnson, J. D. Carbamazepine, a beta-cell protecting drug, reduces type 1 diabetes incidence in NOD mice. *Sci Rep* **8**, 4588, doi:10.1038/s41598-018-23026-w (2018).

22 Catterall, W. A., Goldin, A. L. & Waxman, S. G. International Union of Pharmacology. XLVII. Nomenclature and structure-function relationships of voltage-gated sodium channels. *Pharmacol Rev* **57**, 397-409, doi:10.1124/pr.57.4.4 (2005).

23 Sarmiento, B. E., Santos Menezes, L. F. & Schwartz, E. F. Insulin Release Mechanism Modulated by Toxins Isolated from Animal Venoms: From Basic Research to Drug Development Prospects. *Molecules* **24**, doi:10.3390/molecules24101846 (2019).

24 Zhang, Q. *et al.* Na+ current properties in islet alpha- and beta-cells reflect cell-specific Scn3a and Scn9a expression. *J Physiol* **592**, 4677-4696, doi:10.1113/jphysiol.2014.274209 (2014).

25 Lyon, J. *et al.* Research-Focused Isolation of Human Islets From Donors With and Without Diabetes at the Alberta Diabetes Institute IsletCore. *Endocrinology* **157**, 560-569, doi:10.1210/en.2015-1562 (2016).

26 Ramzy, A. *et al.* AAV8 Ins1-Cre can produce efficient beta-cell recombination but requires consideration of off-target effects. *Sci Rep* **10**, 10518, doi:10.1038/s41598-020-67136-w (2020).

27 Luciani, D. S. & Johnson, J. D. Acute effects of insulin on beta-cells from transplantable human islets. *Mol Cell Endocrinol* **241**, 88-98, doi:10.1016/j.mce.2005.06.006 (2005).

28 Brownrigg, G. P. *et al.* Sex differences in islet stress responses support female beta cell resilience. *Mol Metab* **69**, 101678, doi:10.1016/j.molmet.2023.101678 (2023).

29 Luebbert, L. & Pachter, L. Efficient querying of genomic reference databases with gget. *Bioinformatics* **39**, doi:10.1093/bioinformatics/btac836 (2023).

30 Dai, X. Q. *et al.* SUMOylation regulates insulin exocytosis downstream of secretory granule docking in rodents and humans. *Diabetes* **60**, 838-847, doi:10.2337/db10-0440 (2011).

31 Gopel, S. O. *et al.* Regulation of glucagon release in mouse -cells by KATP channels and inactivation of TTX-sensitive Na+ channels. *J Physiol* **528**, 509-520, doi:10.1111/j.1469-7793.2000.00509.x (2000).

32 Dai, X. Q. *et al.* SUMO1 enhances cAMP-dependent exocytosis and glucagon secretion from pancreatic alpha-cells. *J Physiol* **592**, 3715-3726, doi:10.1113/jphysiol.2014.274084 (2014).

33 Johnson, J. D. *et al.* Different effects of FK506, rapamycin, and mycophenolate mofetil on glucose-stimulated insulin release and apoptosis in human islets. *Cell Transplant* **18**, 833-845, doi:10.3727/096368909X471198 (2009).

34 Lincez, P. J., Shanina, I. & Horwitz, M. S. Reduced expression of the MDA5 Gene IFIH1 prevents autoimmune diabetes. *Diabetes* **64**, 2184-2193, doi:10.2337/db14-1223 (2015).

35 Dobin, A. *et al.* STAR: ultrafast universal RNA-seq aligner. *Bioinformatics* **29**, 15-21, doi:10.1093/bioinformatics/bts635 (2013).

36 Love, M. I., Huber, W. & Anders, S. Moderated estimation of fold change and dispersion for RNA-seq data with DESeq2. *Genome Biol* **15**, 550, doi:10.1186/s13059-014-0550-8 (2014).

37 Wu, T. *et al.* clusterProfiler 4.0: A universal enrichment tool for interpreting omics data. *Innovation (Camb)* **2**, 100141, doi:10.1016/j.xinn.2021.100141 (2021).

38 Szabat, M. *et al.* High-content screening identifies a role for Na(+) channels in insulin production. *R Soc Open Sci* **2**, 150306, doi:10.1098/rsos.150306 (2015).

39 Gwiazda, K. S., Yang, T. L., Lin, Y. & Johnson, J. D. Effects of palmitate on ER and cytosolic Ca2+ homeostasis in beta-cells. *Am J Physiol Endocrinol Metab* **296**, E690-701, doi:10.1152/ajpendo.90525.2008 (2009).

40 Vignali, S., Leiss, V., Karl, R., Hofmann, F. & Welling, A. Characterization of voltage-dependent sodium and calcium channels in mouse pancreatic A- and B-cells. *J Physiol* **572**, 691-706, doi:10.1113/jphysiol.2005.102368 (2006).

41 Chen, C. *et al.* Voltage-Gated Na+ Channels are Modulated by Glucose and Involved in Regulating Cellular Insulin Content of INS-1 Cells. *Cell Physiol Biochem* **45**, 446-457, doi:10.1159/000486921 (2018).

42 Skovso, S. *et al.* beta-Cell Cre Expression and Reduced Ins1 Gene Dosage Protect Mice From Type 1 Diabetes. *Endocrinology* **163**, doi:10.1210/endocr/bqac144 (2022).

43 Yang, C. H. *et al.* Neuropeptide Y1 receptor antagonism protects beta-cells and improves glycemic control in type 2 diabetes. *Mol Metab* **55**, 101413, doi:10.1016/j.molmet.2021.101413 (2022).

44 Rodnoi, P. *et al.* Neuropeptide Y expression marks partially differentiated β cells in mice and humans. *JCI Insight* **2**, doi:10.1172/jci.insight.94005 (2017).

45 Marohnic, C. C. *et al.* Human cytochrome P450 oxidoreductase deficiency caused by the Y181D mutation: molecular consequences and rescue of defect. *Drug Metab Dispos* **38**, 332-340, doi:10.1124/dmd.109.030445 (2010).

46 Zhang, T. *et al.* Recent progress on bioinformatics, functional genomics, and metabolomics research of cytochrome P450 and its impact on drug discovery. *Curr Top Med Chem* **12**, 1346-1355, doi:10.2174/156802612801319052 (2012).

47 Albani, F., Riva, R. & Baruzzi, A. Carbamazepine clinical pharmacology: a review. *Pharmacopsychiatry* **28**, 235-244, doi:10.1055/s-2007-979609 (1995).

48 Dufer, M., Horth, K., Krippeit-Drews, P. & Drews, G. The significance of the nuclear farnesoid X receptor (FXR) in beta cell function. *Islets* **4**, 333-338, doi:10.4161/isl.22383 (2012).

49 Baba, K., Morimoto, H. & Imaoka, S. Seven in absentia homolog 2 (Siah2) protein is a regulator of NF-E2-related factor 2 (Nrf2). *J Biol Chem* **288**, 18393-18405, doi:10.1074/jbc.M112.438762 (2013).

50 Guidry, P. A. & Stroynowski, I. The murine family of gut-restricted class Ib MHC includes alternatively spliced isoforms of the proposed HLA-G homolog, "blastocyst MHC". *J Immunol* **175**, 5248-5259, doi:10.4049/jimmunol.175.8.5248 (2005).

51 Porsche, C. E., Delproposto, J. B., Patrick, E., Zamarron, B. F. & Lumeng, C. N. Adipose tissue dendritic cell signals are required to maintain T cell homeostasis and obesity-induced expansion. *Mol Cell Endocrinol* **505**, 110740, doi:10.1016/j.mce.2020.110740 (2020).

52 Hermel, E., Yuan, J. & Monaco, J. J. Characterization of polymorphism within the H2-M MHC class II loci. *Immunogenetics* **42**, 136-142, doi:10.1007/BF00178588 (1995).

53 Chaparro, R. J. *et al.* Nonobese diabetic mice express aspects of both type 1 and type 2 diabetes. *Proc Natl Acad Sci U S A* **103**, 12475-12480, doi:10.1073/pnas.0604317103 (2006).

54 Zakharov, P. N., Hu, H., Wan, X. & Unanue, E. R. Single-cell RNA sequencing of murine islets shows high cellular complexity at all stages of autoimmune diabetes. *J Exp Med* **217**, doi:10.1084/jem.20192362 (2020).

55 Wieczorek, M. *et al.* Major Histocompatibility Complex (MHC) Class I and MHC Class II Proteins: Conformational Plasticity in Antigen Presentation. *Front Immunol* **8**, 292, doi:10.3389/fimmu.2017.00292 (2017).

56 Chen, S. Y. *et al.* Investigating the Expression and Function of the Glucose Transporter GLUT6 in Obesity. *Int J Mol Sci* **23**, doi:10.3390/ijms23179798 (2022).

57 Fridlyand, L. E., Jacobson, D. A. & Philipson, L. H. Ion channels and regulation of insulin secretion in human beta-cells: a computational systems analysis. *Islets* **5**, 1-15, doi:10.4161/isl.24166 (2013).

58 Martin, G. M., Chen, P. C., Devaraneni, P. & Shyng, S. L. Pharmacological rescue of trafficking-impaired ATP-sensitive potassium channels. *Front Physiol* **4**, 386, doi:10.3389/fphys.2013.00386 (2013).

59 Callaway, J. K., Beart, P. M., Jarrott, B. & Giardina, S. F. Incorporation of sodium channel blocking and free radical scavenging activities into a single drug, AM-36, results in profound inhibition of neuronal apoptosis. *Br J Pharmacol* **132**, 1691-1698, doi:10.1038/sj.bjp.0704018 (2001).

60 Cardoso, F. C. *et al.* Identification and Characterization of ProTx-III [mu-TRTX-Tp1a], a New Voltage-Gated Sodium Channel Inhibitor from Venom of the Tarantula Thrixopelma pruriens. *Mol Pharmacol* **88**, 291-303, doi:10.1124/mol.115.098178 (2015).

61 Gaida, W., Klinder, K., Arndt, K. & Weiser, T. Ambroxol, a Nav1.8-preferring Na(+) channel blocker, effectively suppresses pain symptoms in animal models of chronic, neuropathic and inflammatory pain. *Neuropharmacology* **49**, 1220-1227, doi:10.1016/j.neuropharm.2005.08.004 (2005).

62 Sheets, P. L., Heers, C., Stoehr, T. & Cummins, T. R. Differential block of sensory neuronal voltage-gated sodium channels by lacosamide [(2R)-2-(acetylamino)-N-benzyl-3-methoxypropanamide], lidocaine, and carbamazepine. *J Pharmacol Exp Ther* **326**, 89-99, doi:10.1124/jpet.107.133413 (2008).

63 Leung, Y. M. *et al.* Electrophysiological characterization of pancreatic islet cells in the mouse insulin promoter-green fluorescent protein mouse. *Endocrinology* **146**, 4766-4775, doi:10.1210/en.2005-0803 (2005).

64 Nita, II *et al.* Pancreatic beta-cell Na+ channels control global Ca2+ signaling and oxidative metabolism by inducing Na+ and Ca2+ responses that are propagated into mitochondria. *FASEB J* **28**, 3301-3312, doi:10.1096/fj.13-248161 (2014).

65 Kim, W. H. *et al.* Exposure to chronic high glucose induces beta-cell apoptosis through decreased interaction of glucokinase with mitochondria: downregulation of glucokinase in pancreatic beta-cells. *Diabetes* **54**, 2602-2611, doi:10.2337/diabetes.54.9.2602 (2005).

66 Banday, M. Z., Sameer, A. S. & Nissar, S. Pathophysiology of diabetes: An overview. *Avicenna J Med* **10**, 174-188, doi:10.4103/ajm.ajm_53_20 (2020).

67 Wang, Z., York, N. W., Nichols, C. G. & Remedi, M. S. Pancreatic beta cell dedifferentiation in diabetes and redifferentiation following insulin therapy. *Cell Metab* **19**, 872-882, doi:10.1016/j.cmet.2014.03.010 (2014).

68 Dong, X. X., Wang, Y. & Qin, Z. H. Molecular mechanisms of excitotoxicity and their relevance to pathogenesis of neurodegenerative diseases. *Acta Pharmacol Sin* **30**, 379-387, doi:10.1038/aps.2009.24 (2009).

69 Poitout, V. *et al.* Glucolipotoxicity of the pancreatic beta cell. *Biochim Biophys Acta* **1801**, 289-298, doi:10.1016/j.bbalip.2009.08.006 (2010).

70 Grill, V. & Bjorklund, A. Overstimulation and beta-cell function. *Diabetes* **50 Suppl 1**, S122-124, doi:10.2337/diabetes.50.2007.s122 (2001).

71 Khaldi, M. Z., Guiot, Y., Gilon, P., Henquin, J. C. & Jonas, J. C. Increased glucose sensitivity of both triggering and amplifying pathways of insulin secretion in rat islets cultured for 1 wk in high glucose. *Am J Physiol Endocrinol Metab* **287**, E207-217, doi:10.1152/ajpendo.00426.2003 (2004).

72 Fischer, L., Scherbarth, F., Chagnaud, B. & Felmy, F. Intrinsic frequency response patterns in mechano-sensory neurons of the leech. *Biol Open* **6**, 993-999, doi:10.1242/bio.023960 (2017).

73 Jo, S. & Bean, B. P. Sidedness of carbamazepine accessibility to voltage-gated sodium channels. *Mol Pharmacol* **85**, 381-387, doi:10.1124/mol.113.090472 (2014).

74 Isam Hamo Mahmood, Z. K. M. Effects of Carbamazepine on blood pressure, serum glucose concentration, lipid profile and prevalence of metabolic syndrome in epileptic patients. *Tikrit Journal of Pharmaceutical Sciences* (2012).

75 Sreenan, S. *et al.* Increased beta-cell proliferation and reduced mass before diabetes onset in the nonobese diabetic mouse. *Diabetes* **48**, 989-996, doi:10.2337/diabetes.48.5.989 (1999).

76 Moriyama, H. *et al.* Evidence for a primary islet autoantigen (preproinsulin 1) for insulitis and diabetes in the nonobese diabetic mouse. *Proc Natl Acad Sci U S A* **100**, 10376-10381, doi:10.1073/pnas.1834450100 (2003).

77 Kikutani, H. & Makino, S. The murine autoimmune diabetes model: NOD and related strains. *Adv Immunol* **51**, 285-322, doi:10.1016/s0065-2776(08)60490-3 (1992).

78 Bach, J. F. Insulin-dependent diabetes mellitus as an autoimmune disease. *Endocr Rev* **15**, 516-542, doi:10.1210/edrv-15-4-516 (1994).

79 Serreze, D. V. *et al.* Diabetes acceleration or prevention by a coxsackievirus B4 infection: critical requirements for both interleukin-4 and gamma interferon. *J Virol* **79**, 1045-1052, doi:10.1128/JVI.79.2.1045-1052.2005 (2005).

Figure Legends

Figure 1. **Na^+ channel inhibitors reduced cytokine-induced cell death in human islets. (A-E)** Dispersed islet cells, seeded into 384-well plates and stained with Hoechst and PI, were treated with a cytokine cocktail or 1 μM thapsigargin, in combination with either 0.0 to 200 μM concentrations of Na^+ channel inhibitors carbamazepine **(A)**, ambroxol **(E)** or 0.001 to 1 μM of oxcarbazepine **(B)** and spider toxin ProTxII **(C)** and Na^+ channel enhancer **(D)** veratridine. Dimethyl sulfoxide (DMSO)-treated islets were used as the control and the same results are shown in each panel. Cells were imaged with ImageXpress Micro and the percentage of PI-positive (PI+) cells was calculated. *Insets* represent quantification of cell death at 72h time point (n = 3-18 human islet cell cultures, similar results were observed across human islet cultures from 4 donors). *p<0.05. Data were evaluated using 1-way ANOVA with Šídák's multiple comparisons test and is significant different from the respectable control (Black).

Figure 2. Glucose dependent insulin secretion in the presences of Na^+ channel inhibitors and enhancers. (A-F) 65 human islets were perifused with Krebs-Ringer bicarbonate buffer containing 3 mM or 15 mM glucose (grey line) or 30 mM KCl (red line) in combination with 20 μM carbamazepine **(A)**, 0.1 μM oxcarbazepine **(B)**, 0.1 μM ProTxII spider toxin **(C)**, 20 μM ambroxol **(D)** and 20 μM veratridine **(E)**. Quantification of area under the curve (AUC) of 15mM glucose and 30 mM KCl phase from figure A-F **(F)**. (n = 6, mean ± SEM, p value shown). DMSO, dimethyl sulfoxide, mean from corresponding control from each specific run. AUC data were evaluated using 2-way ANOVA with multiple comparison (mixed models) with Dunnett correction for multiple comparisons.

Figure 3. Voltage-gated Na^+ channel alpha subunit gene expression in single human and mouse islet cells. (**A,B)** Human and mouse islet cell scRNA data were visualized after extraction from the CELLxGENE Discover Census as described in the Methods.

Figure 4. Scn9a-deficient β-cells had reduced Na+ current. (A) Breeding strategy and structure of the wildtype (WT) *Ins1* locus, recombinant alleles result of targeting vector *Ins1* Cre locus (Cre), *Scn9a* WT locus and *Scn9a* floxed gene (flox). Created with Biorender.com. **(B)** Fluorescent imaging of *Scn9a* expression of β-cell from NOD mice. Representative images a 20x objective. Cells immune stained for Insulin (magenta) with *Scn9a* (green). **(C)** Representative Na^+ current traces recorded from β-cells with 2.6 mM Ca^{2+} in the extracellular solution. **(D)** Peak Na^+ current normalized to cell size (pA/pF) as a function of voltage. **(E,F)** Representative Ca^{2+} currents and quantification. **(G)** Membrane potential recording from β-cells exposed to 6 mM, 3 mM, or 12 mM glucose. **(H-J)** Action potential (AP) frequency, threshold and height were measured at 6 mM or 12 mM glucose in β-cells. All experiments were done

in 18-week-old mice. Wildtype shown in black, female shown in blue and male mice in green. Heterozygous (HET) mice shown in brown. Statistics performed were unpaired t test.

Figure 5. Reduced glucose stimulated insulin secretion from *Scn9a*-deficient β-cells. (A,B) Glucose-dependent insulin secretion from 100 whole mouse islets, perifused with Krebs-Ringer bicarbonate buffer containing 3, 6, 9 and 15 mM glucose delivered in a ramp-like manner and repeated with or without 20 mM carbamazepine (indicated by dotted line -b) or 30 mM KCl (red line -c) (normalized to baseline at 3 mM glucose). Inserts represent quantification of area under the curve (AUC) of KCl (c), glucose ramp phase (a and b) or each individual ramp phase. (n = 6). **(C)** Changes in the 340/380 nm Fura-2 ratio measured Scn9a-deficient dispersed β-cell perifused with Krebs-Ringer bicarbonate buffer containing 3, 6, 9, 15 mM glucose delivered in a ramp-like manner (grey box) or 30 mM KCl (red line). Inserts represent quantification of AUC of KCl or individual glucose ramp phase. Each glucose ramp phase was normalized to baseline (3 mM glucose) (n = 4-5). **(D)** Glucose-dependent exocytotic responses β-cells measured as increases in cell membrane capacitance by whole-cell patch clamp at 5 mM glucose (n = 3-5). Wildtype mice shown in black, female mice are shown in blue and male in green, experiments were done in 18-week-old mice. **(C)** AUC data were evaluated using 2-way ANOVA with multiple comparison (mixed models) with Dunnett correction for multiple comparisons.

Figure 6. Carbamazepine reduces cell death through *Scn9a*. (A) Dispersed islet cells from 18 weeks old male, wildtype and *Scn9a* knockout mice seeded onto 384-well plate were stained with Hoechst and PI. Cells were treated with a cytokine cocktail or 1 μM thapsigargin, in combination with either to 20 μM carbamazepine, veratridine or DMSO. Cells were imaged with ImageXpress^{MICRO} and the percentage of PI-positive (PI+) cells was calculated and represents quantification of cell death at 72 h time point (n = 4 islet cell culture from each of 4 mice). Data were evaluated using 1-way ANOVA with Šídák's multiple comparisons test.

Figure 7. *Scn9a* deletion did not change diabetes incidence or glucose tolerance in NOD mice lacking 1 allele of *Ins1*. (A,B) Kaplan-Meier plot denoting diabetes incidence in NOD mice from male (green), female (blue), wildtype, and *Scn9a* knock-out mice. Grey represents female mice that are fully wildtype, with both Ins1 alleles intact (n = 12-13). Survival analysis was performed using Log-rank (Mantel-Cox) test *p<0.05. **(C)** Example key for insulitis scoring, showing 0 – no insulitis, 1 – peri-insulitis (<25% peripheral immune invasion), 2 – insulitis (25-75% immune invasion), 3 – severe insulitis (>75%). Insulitis scoring data using the H&E scoring model for NOD mice at 18-weeks (n=5-6). **(D)** Examples of islets stained for insulin, used for the insulin-stain insulitis scoring method. The islet periphery is outlined in red and yellow (i represent after analysis and ii before, while a-c represents increasing severity of insulitis, respectively). **(E)** Violin plot showing the insulitis proportion using the insulin stain scoring model

in 18-week old NOD mice (n =6). **(F-I)** *In vivo* insulin secretion and glucose tolerance tests in NOD mice by intraperitoneally injection (IP) with 2 g/kg of glucose in 18-week old NOD mice. **(F,H)** Blood was collected at 0 minutes (baseline), at 15 for *in vivo* insulin section. **(G,I)** Blood glucose was measured as 0, 15, 30, 60 and 120 minutes, after injection. Inserts represent of area under the curve (AUC) (n=7-10). **(J)** Representative apoptotic cell death images used for quantification via TUNEL staining **(K)** in the pre-diabetic NOD mice (n = 7). **(L)** Representative example of proliferating islet cells and close-up images showing example of a proliferating β-cell (i,ii), i shows proliferating example and ii non. **(M)** In the pre-diabetic NOD mice (n = 4-5). **(O)** Representative images for insulin intensity and islet size used for quantified via insulin stain, **(N)** in the pre-diabetic NOD mice. **(Q)** β-cell area was quantified via insulin staining in NOD mice (n = 5-7). **(R)** Insulin content in whole islets from male NOD mice (n = 5-7). *p<0.05. **(E)** Data were evaluated using Nested one-way ANOVA. **(F,G,Q and R)** One-way ANOVA.

Figure 8. *Scn9a* deletion using AAV8-Cre virus protects NOD mice from type 1 diabetes. (A) Study design shown as schematic diagram of experiments conducted on NOD mice. **(B)** Efficiency of AAV8-Ins1 virus in female NOD mice is illustrated using 1×10^{12} VGP of virus carrying GFP instead of Cre, 4 weeks post injection. **(C)** Kaplan-Meier plot denoting diabetes incidence in female NOD wildtype (receiving AAV8-*ins1*-Cre), wildtype without AAV8 injected (grey dotted line, from *Ins1*Cre cohort shown in figure.6A.) and *Scn9a* knock out mice (n = 7-16). Mice were administered 1×10^{12} VGP AAV8 *Ins1*-Cre by intraperitoneal injection (IP) at 6-7 weeks indicated by arrow. Survival analysis was performed using Log-rank (Mantel-Cox) test. **(D,E)** *In vivo* insulin secretion and glucose tolerance tests in NOD mice by intraperitoneally injection (IP) with 2 g/kg of glucose in 12-week old NOD mice. **(D)** Blood was collected at 0 minutes (baseline), at 15 for *in vivo* insulin section. **(E)** Blood glucose was measured as 0, 15, 30, 60 and 120 minutes, after injection. *Insert* represents of area under the curve (AUC) (n = 9-10). **(F)** Violin plot showing the insulitis proportion in 12-week-old mice. **(G)** Insulin staining intensity quantified as a percentage of insulin positive area in 12-week-old mice (n= 6-7). **(H)** Insulin-positive cell area, as a percentage of total pancreas area, in 12-week-old mice (n= 6-7). *p<0.05. **(D and E)** Data were evaluated using one-way ANOVA.

Figure 9. RNA-seq data from male *Scn9a* KO NOD mouse islets show differentially expressed genes. (B-D) mRNAs that were nominally differentially expressed in islets between wildtype (WT), heterozygous (HET) and complete Scn9a knock outs (KO) in male mice at 18 weeks of age. **(A)** Quantification of *Scn9a* exon 3 (Floxed part of the *Scn9a* gene) counts from scRNA-seq analysis between genotypes. **(B)** Identified differentially expressed mRNAs with blue dots represent downregulated and red dots represent upregulated genes. **(C)** All transcripts of significantly differentially expressed genes **(D).** Top significantly enriched Reactome pathways from the top significantly differentially expressed genes. Gene Ontology (GO) Molecular Function (MF) database. (n= 4-5).

Supplementary Figures

Figure S1. Heterozygous *Scn9a* knockout mice have reduced glucose stimulated insulin secretion. (A) Membrane potential recording from β-cell exposed to 6,3 and 12 mM glucose. **(B)** Action potential (AP) frequency, threshold and height were measured at 6 mM and 12 mM glucose in β-cells. **(C)** Changes in the 340/380 nm Fura-2 ratio measured Scn9a-deficient dispersed β-cell perifused with Krebs-Ringer bicarbonate buffer containing 3,6,9 and15 mM glucose in ramp like manner (Grey box) or 30 mM KCl (red line). Inserts represent quantification of AUC of KCl or individual glucose ramp phase. Each glucose ramp phase was normalized to baseline (3 mM glucose) (n = 4-5). **(D,E)** Glucose dependent Insulin secretion from 100 whole mouse, perifused with Krebs-Ringer bicarbonate buffer containing 3,6,9 and15 mM glucose in ramp like manner repeated with or without 20 mM of carbamazepine (indicated by dotted line -b) or 30 mM KCl (red line -c) (Normalized to baseline at 3 mM glucose). Inserts represent quantification of rea under the curve (AUC) of KCl (c), glucose ramp phase (a and b) or each individual ramp phase. (n = 6). **(F)** Glucose-depended exocytotic responses β-cells measured as increases in cell membrane capacitance by whole-cell patch clamp at 5mM glucose. (n = 3-5). **(C)** AUC data were evaluated using 2-way ANOVA with multiple comparison (mixed models) with Dunnett correction for multiple comparisons. **(F)** Nested one-way ANOVA.

Figure S2. Heterozygous *Scn9a* knock out mice demonstrate a worsening in glucose tolerance. (A-D) In vivo insulin section and glucose tolerance tests in NOD mice by intraperitoneally injection (IP) with 2g/kg of glucose at 18-weeks of age. **(A,C)** Blood was collected at 0 minutes (baseline), at 15 for in vivo insulin section. **(B,D)** Blood glucose was measured as 0, 15, 30, 60 and 120 minutes, after injection. Insert represents of area under the curve (AUC) (n = 9). **(E,F)** Kaplan-Meier plot denoting diabetes incidence in NOD mice from male and female NOD mice (n = 12-13). Survival analysis was performed using Log-rank (Mantel-Cox) test. (mean ± SEM, p value shown). Wildtype in black, female in blue and male mice shown in brown. *p<0.05. **(A-D)** Data were evaluated using 1-way ANOVA.

Figure S3. Heterozygous *Scn9a* knock out mice is not protected from diabetes. (A) Kaplan-Meier plot denoting diabetes incidence in female NOD wildtype and heterozygous *Scn9a* knock out mice (n = 11-15). Mice were administered 1×10^{12} VGP AAV8 Ins1-Cre intraperitoneal injection (IP) at 6-7 weeks indicated by red arrow. Survival analysis was performed using Log-rank (Mantel-Cox) test. **(B,C)** In vivo insulin section and glucose tolerance tests in NOD mice by intraperitoneally injection (IP) with 2g/kg of glucose at 12-weeks of age. **(B)** Blood was collected at 0 minutes (baseline), at 15 for in vivo insulin section. **(C)** Blood glucose was measured as 0, 15, 30, 60 and 120 minutes, after injection. Insert represents of area under the curve (AUC) (n 9-10). **(D)** Violin plot showing the insulitis proportion using the insulin stain scoring model for 12-weeks old NOD mice. **(E)** β-cell area was quantified via insulin staining in 12 weeks old mice NOD mice (n = 6). Wildtype mice shown in black and heterozygous knock

out mice in red. *p<0.05. **(D)** Data were evaluated using Nested one-way ANOVA. **(A-C and D)** One-way ANOVA.

Figure S4. Heterozygous *Scn9a* knock out mice have increased islet apoptosis and are not protected from ER- and cytokine-induced cell death. (A) Dispersed islet cells from male, wildtype and heterozygous Scn9a knock out mice seeded onto 384-well plate were stained with Hoechst and PI. Cells were treated with a cytokine cocktail or 1 μM thapsigargin, in combination with either to 20 μM Carbamazepine, Veratridine or DMSO, dimethyl sulfoxide. Cells were imaged with ImageXpress Micro and the percentage of PI-positive (PI+) cells was calculated and represents quantification of cell death at 72h time point**. (B)** Representative apoptotic cell death images used for quantification via TUNEL staining (i represent after analysis and ii before, while a-b represent increasing severity of insulitis), in the pre-diabetic NOD mice (n=9). **(C,D)** β-cell area was quantified via insulin staining in NOD mice (n = 6-7). Insulin content in whole islets from male NOD mice (n = 5-7) **(D)**. All experiments were carried out in 18-week old mice. **(A)** Data were evaluated using 1-way ANOVA with Šídák's multiple comparisons test. **(B-D)** One-way ANOVA.

Figure 1

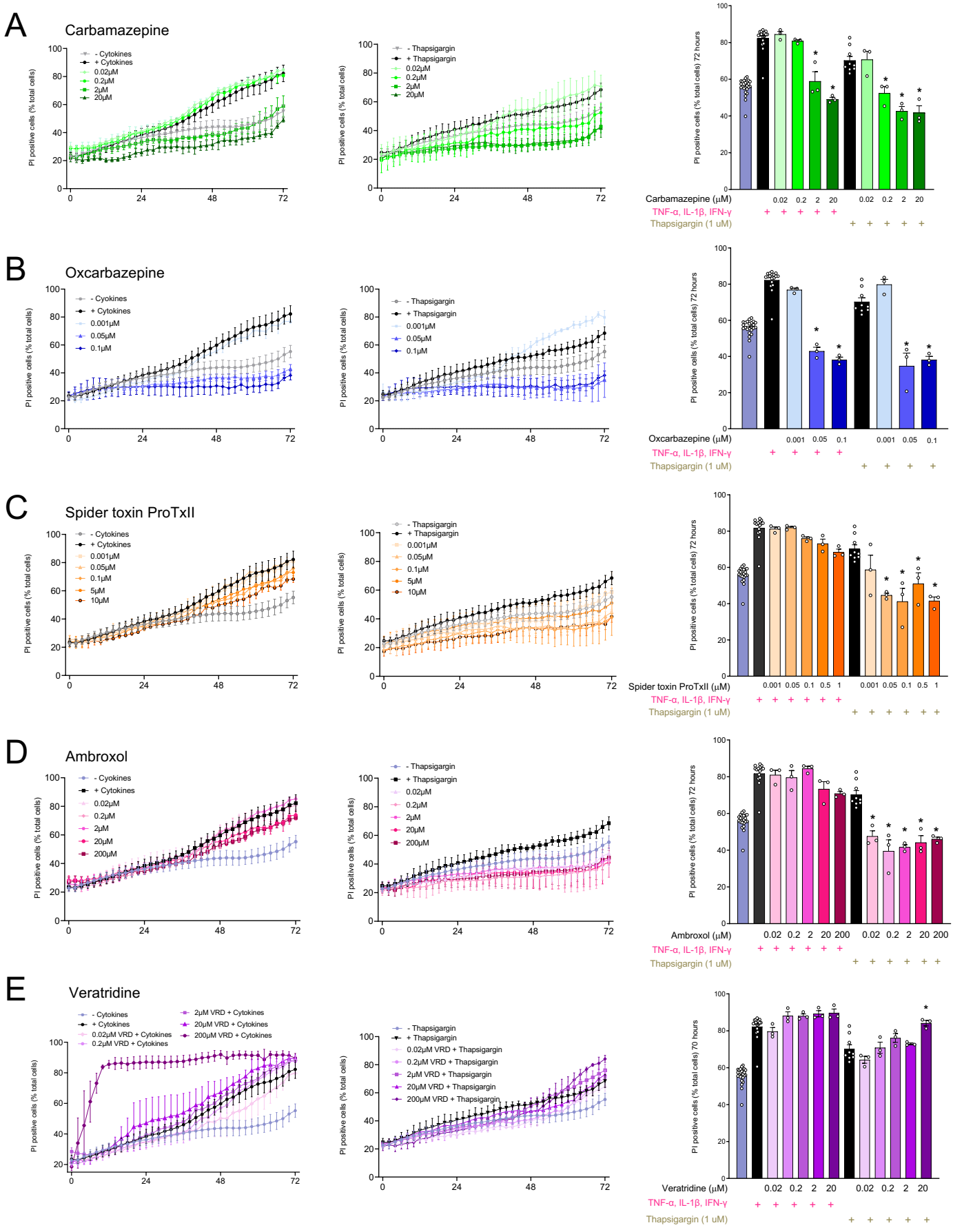
A
Carbamazepine
- Cytokines
+ Cytokines
0.02μM
0.2μM
2μM
20μM
- Thapsigargin
+ Thapsigargin
PI positive cells (% total cells)
PI positive cells (% total cells) 72 hours
Carbamazepine (μM)
0.02 0.2 2 20 0.02 0.2 2 20
TNF-α, IL-1β, IFN-γ
Thapsigargin (1 uM)
B
Oxcarbazepine
0.001μM
0.05μM
0.1μM
Oxcarbazepine (μM)
0.001 0.05 0.1 0.001 0.05 0.1
C
Spider toxin ProTxII
5μM
10μM
Spider toxin ProTxII (μM)
0.001 0.05 0.1 0.5 1 0.001 0.05 0.1 0.5 1
D
Ambroxol
200μM
Ambroxol (μM)
0.02 0.2 2 20 200 0.02 0.2 2 20 200
E
Veratridine
2μM VRD + Cytokines
20μM VRD + Cytokines
200μM VRD + Cytokines
0.02μM VRD + Cytokines
0.2μM VRD + Cytokines
0.02μM VRD + Thapsigargin
0.2μM VRD + Thapsigargin
2μM VRD + Thapsigargin
20μM VRD + Thapsigargin
200μM VRD + Thapsigargin
PI positive cells (% total cells) 70 hours
Veratridine (μM)
0.02 0.2 2 20 0.02 0.2 2 20

Figure 2

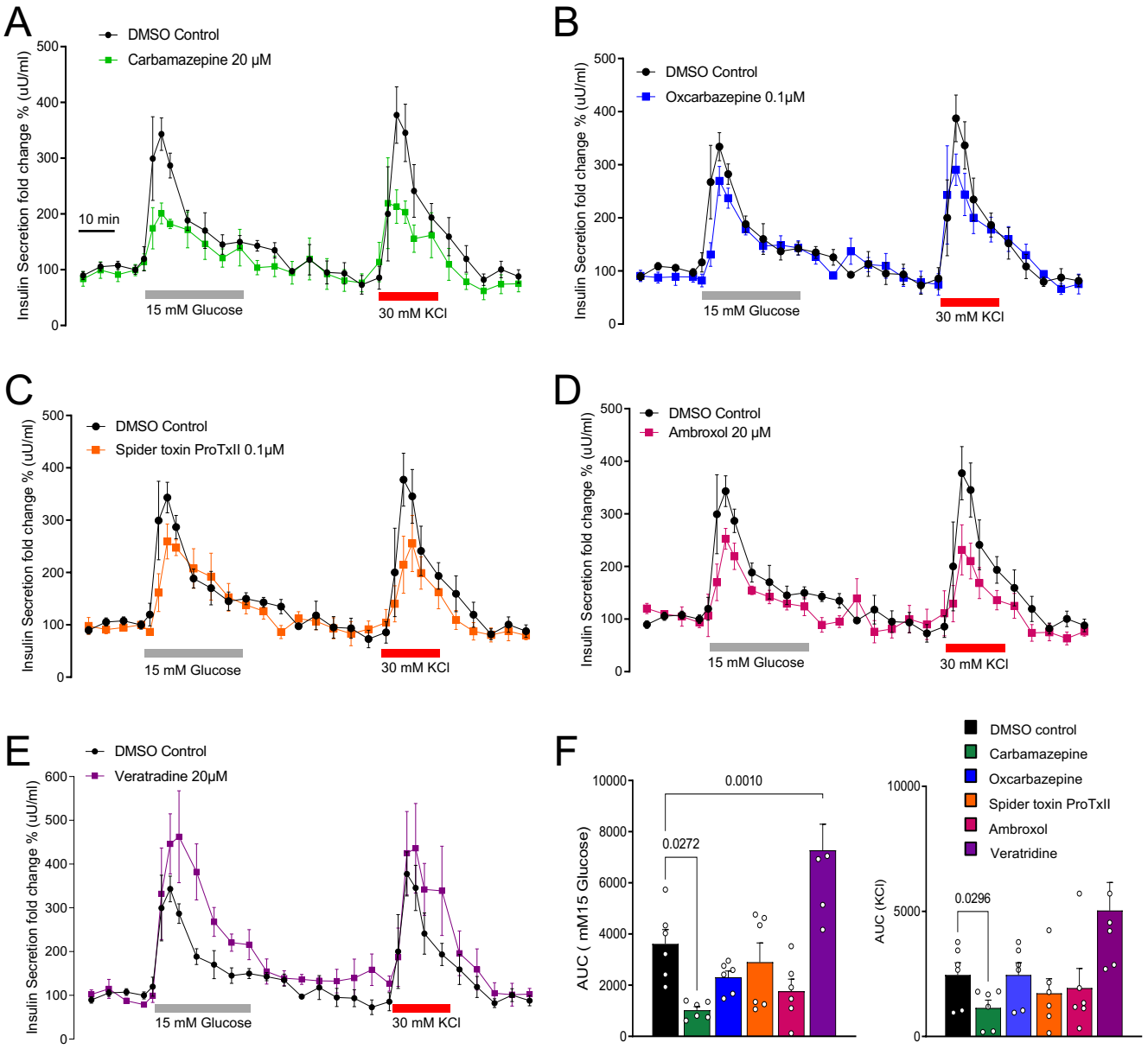
A
DMSO Control
Carbamazepine 20 μM
Insulin Secretion fold change % (uU/ml)
10 min
15 mM Glucose
30 mM KCl
B
DMSO Control
Oxcarbazepine 0.1μM
C
DMSO Control
Spider toxin ProTxII 0.1μM
D
DMSO Control
Ambroxol 20 μM
E
DMSO Control
Veratradine 20μM
F
0.0010
0.0272
AUC (mM15 Glucose)
AUC (KCl)
0.0296
DMSO control
Carbamazepine
Oxcarbazepine
Spider toxin ProTxII
Ambroxol
Veratridine

Figure 3

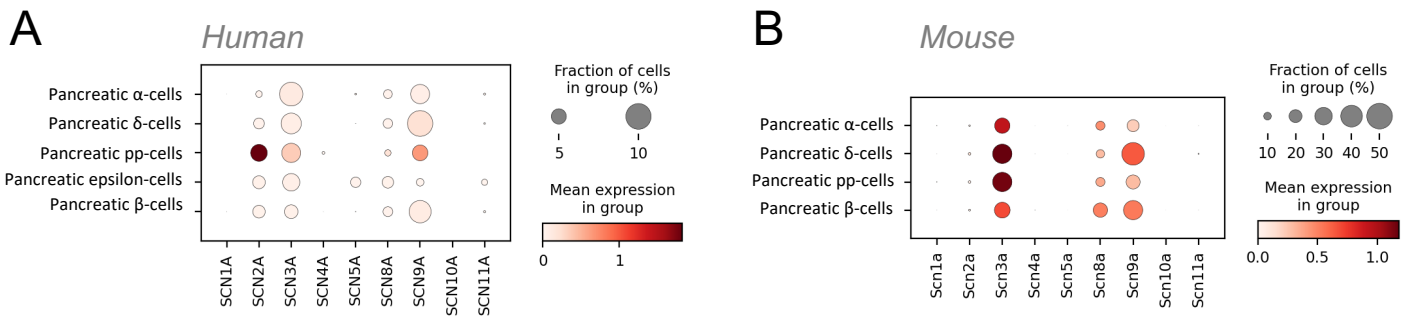
A
Human
Pancreatic α-cells
Pancreatic δ-cells
Pancreatic pp-cells
Pancreatic epsilon-cells
Pancreatic β-cells
SCN1A
SCN2A
SCN3A
SCN4A
SCN5A
SCN8A
SCN9A
SCN10A
SCN11A
Fraction of cells in group (%)
5
10
Mean expression in group
0
1
B
Mouse
Pancreatic α-cells
Pancreatic δ-cells
Pancreatic pp-cells
Pancreatic β-cells
Scn1a
Scn2a
Scn3a
Scn4a
Scn5a
Scn8a
Scn9a
Scn10a
Scn11a
Fraction of cells in group (%)
10
20
30
40
50
Mean expression in group
0.0
0.5
1.0

Figure 4

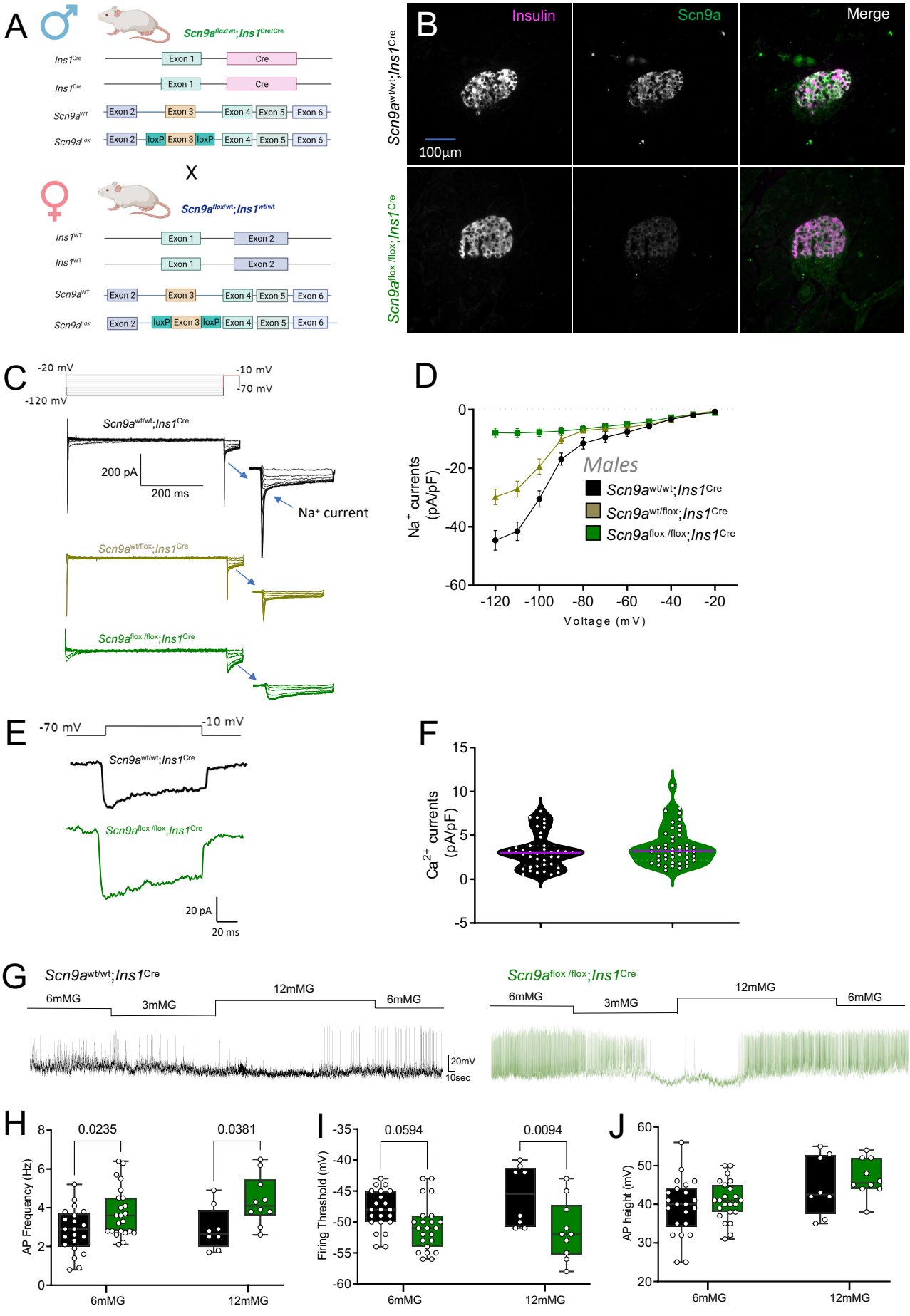
A
Scn9a flox/wt;Ins1 Cre/Cre
Ins1 Cre
Exon 1
Cre
Scn9a WT
Exon 2
Exon 3
Exon 4
Exon 5
Exon 6
Scn9a flox
loxP
X
Scn9a flox/wt;Ins1 wt/wt
Ins1 WT
Exon 1
Exon 2
B
Insulin
Scn9a
Merge
Scn9a wt/wt;Ins1 Cre
Scn9a flox /flox;Ins1 Cre
100µm
C
-20 mV
-10 mV
-70 mV
-120 mV
Scn9a wt/wt;Ins1 Cre
200 pA
200 ms
Na+ current
Scn9a wt/flox;Ins1 Cre
Scn9a flox /flox;Ins1 Cre
D
Na+ currents (pA/pF)
Males
Scn9a wt/wt;Ins1 Cre
Scn9a wt/flox;Ins1 Cre
Scn9a flox /flox;Ins1 Cre
Voltage (mV)
E
-70 mV
-10 mV
Scn9a wt/wt;Ins1 Cre
Scn9a flox /flox;Ins1 Cre
20 pA
20 ms
F
Ca2+ currents (pA/pF)
G
Scn9a wt/wt;Ins1 Cre
Scn9a flox /flox;Ins1 Cre
6mMG
3mMG
12mMG
6mMG
20mV
10sec
H
AP Frequency (Hz)
0.0235
0.0381
6mMG
12mMG
I
Firing Threshold (mV)
0.0594
0.0094
6mMG
12mMG
J
AP height (mV)
6mMG
12mMG

Figure 5

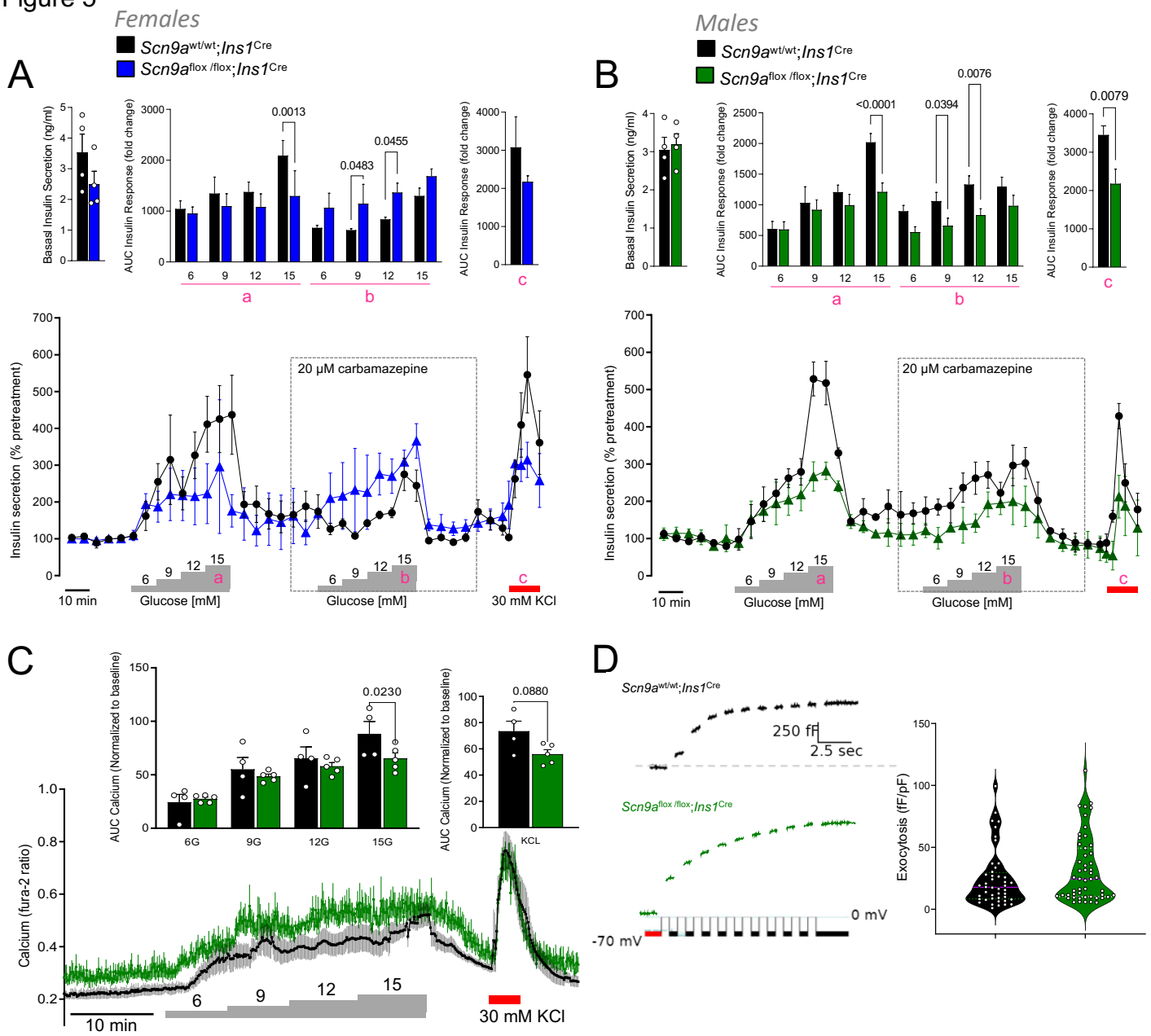
Females
Scn9awt/wt;Ins1Cre
Scn9aflox /flox;Ins1Cre
A
Basal Insulin Secretion (ng/ml)
AUC Insulin Response (fold change)
0.0013
0.0483
0.0455
6 9 12 15 6 9 12 15
a
b
AUC Insulin Response (fold change)
c
Insulin secretion (% pretreatment)
20 μM carbamazepine
6 9 12 15 a
6 9 12 15 b
c
10 min
Glucose [mM]
Glucose [mM]
30 mM KCl
Males
Scn9awt/wt;Ins1Cre
Scn9aflox /flox;Ins1Cre
B
Basal Insulin Secretion (ng/ml)
AUC Insulin Response (fold change)
<0.0001
0.0394
0.0076
6 9 12 15 6 9 12 15
a
b
AUC Insulin Response (fold change)
0.0079
c
Insulin secretion (% pretreatment)
20 μM carbamazepine
6 9 12 15 a
6 9 12 15 b
c
10 min
Glucose [mM]
Glucose [mM]

C
AUC Calcium (Normalized to baseline)
0.0230
6G 9G 12G 15G
AUC Calcium (Normalized to baseline)
0.0880
KCL
Calcium (fura-2 ratio)
6 9 12 15
10 min
30 mM KCl

D
Scn9awt/wt;Ins1Cre
250 fF
2.5 sec
Scn9aflox /flox;Ins1Cre
0 mV
-70 mV
Exocytosis (fF/pF)

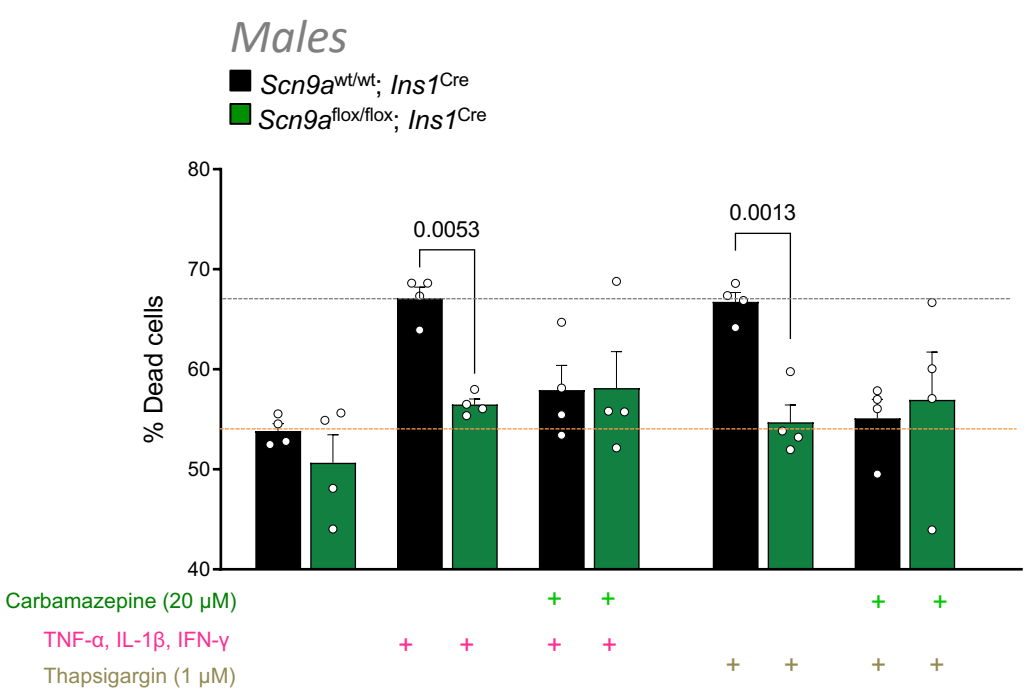
Males
Scn9a wt/wt; Ins1 Cre
Scn9a flox/flox; Ins1 Cre
% Dead cells
80
70
60
50
40
0.0053
0.0013
Carbamazepine (20 µM)
TNF-α, IL-1β, IFN-γ
Thapsigargin (1 µM)

Figure 7

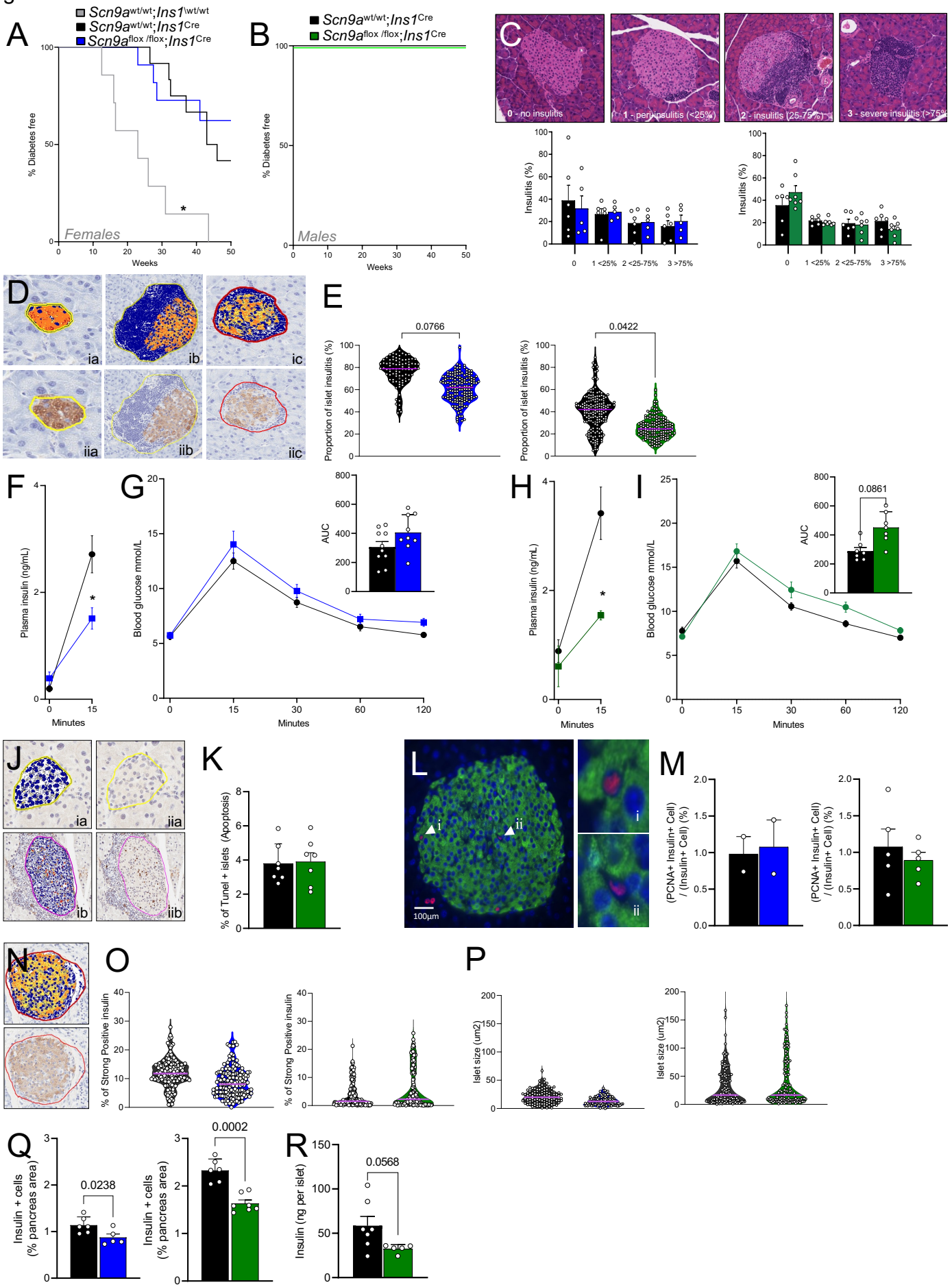
A
Scn9a wt/wt;Ins1 \wt/wt
Scn9a wt/wt;Ins1 Cre
Scn9a flox /flox;Ins1 Cre
% Diabetes free
Weeks
Females
B
Scn9a wt/wt;Ins1 Cre
Scn9a flox /flox;Ins1 Cre
% Diabetes free
Weeks
Males
C
0 - no insulitis
1 - peri-insulitis (<25%)
2 - insulitis (25-75%)
3 - severe insulitis (>75%)
Insulitis (%)
0
1 <25%
2 <25-75%
3 >75%
D
ia
ib
ic
iia
iib
iic
E
0.0766
Proportion of islet insulitis (%)
0.0422
Proportion of islet insulitis (%)
F
Plasma insulin (ng/mL)
Minutes
G
Blood glucose mmol/L
Minutes
AUC
H
Plasma insulin (ng/mL)
Minutes
I
Blood glucose mmol/L
Minutes
AUC
0.0861
J
ia
iia
ib
iib
K
% of Tunel + islets (Apoptosis)
L
i
ii
100µm
M
(PCNA+ Insulin+ Cell) / (Insulin+ Cell) (%)
(PCNA+ Insulin+ Cell) / (Insulin+ Cell) (%)
N
O
% of Strong Positive insulin
% of Strong Positive insulin
P
Islet size (um2)
Islet size (um2)
Q
0.0238
Insulin + cells (% pancreas area)
0.0002
Insulin + cells (% pancreas area)
R
0.0568
Insulin (ng per islet)

Figure 8

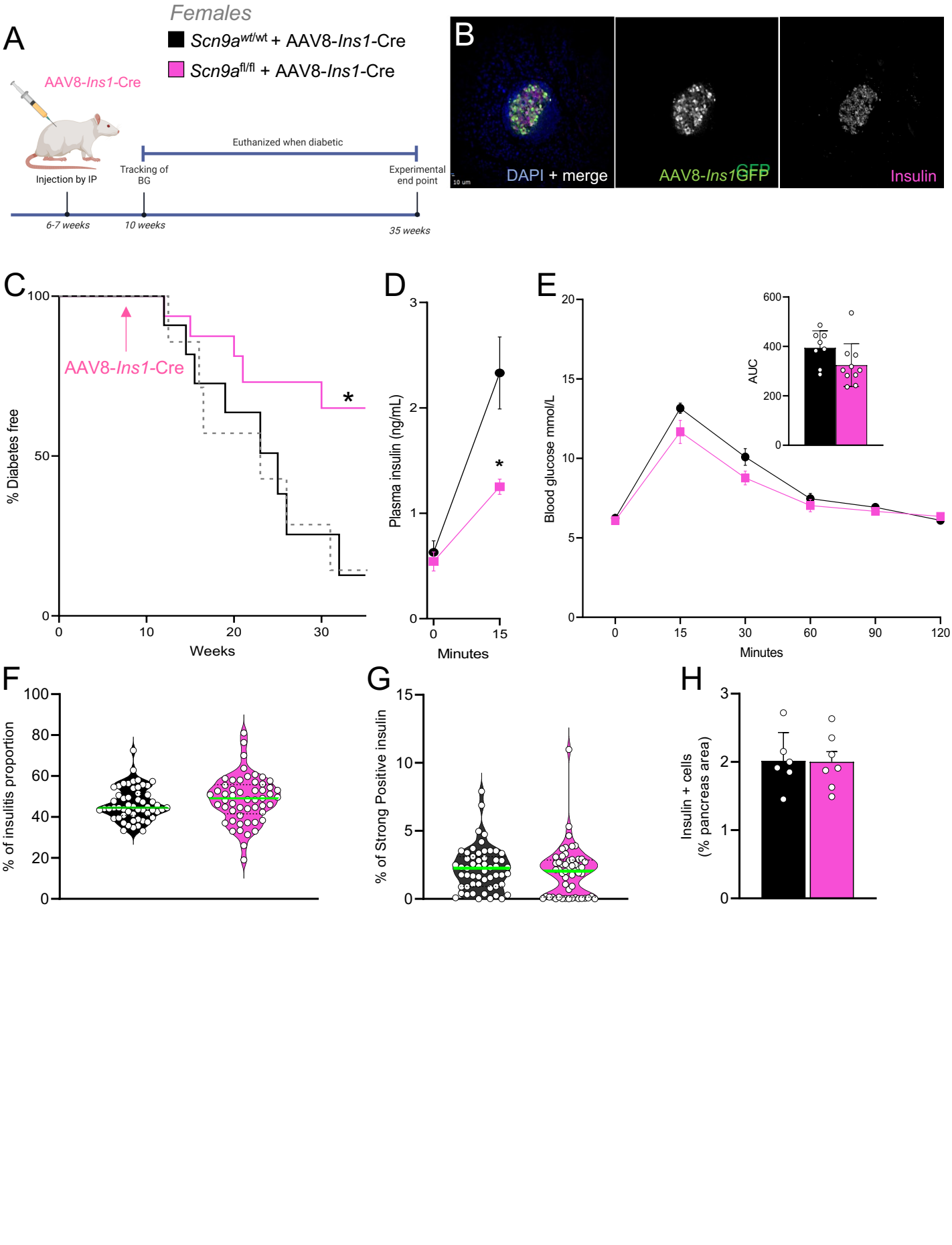
A
Females
Scn9a wt/wt + AAV8-Ins1-Cre
Scn9a fl/fl + AAV8-Ins1-Cre
AAV8-Ins1-Cre
Injection by IP
Tracking of BG
Euthanized when diabetic
Experimental end point
6-7 weeks
10 weeks
35 weeks
B
DAPI + merge
AAV8-Ins1GFP
Insulin
C
% Diabetes free
AAV8-Ins1-Cre
Weeks
D
Plasma insulin (ng/mL)
Minutes
E
Blood glucose mmol/L
AUC
Minutes
F
% of insulitis proportion
G
% of Strong Positive insulin
H
Insulin + cells (% pancreas area)

Figure 9

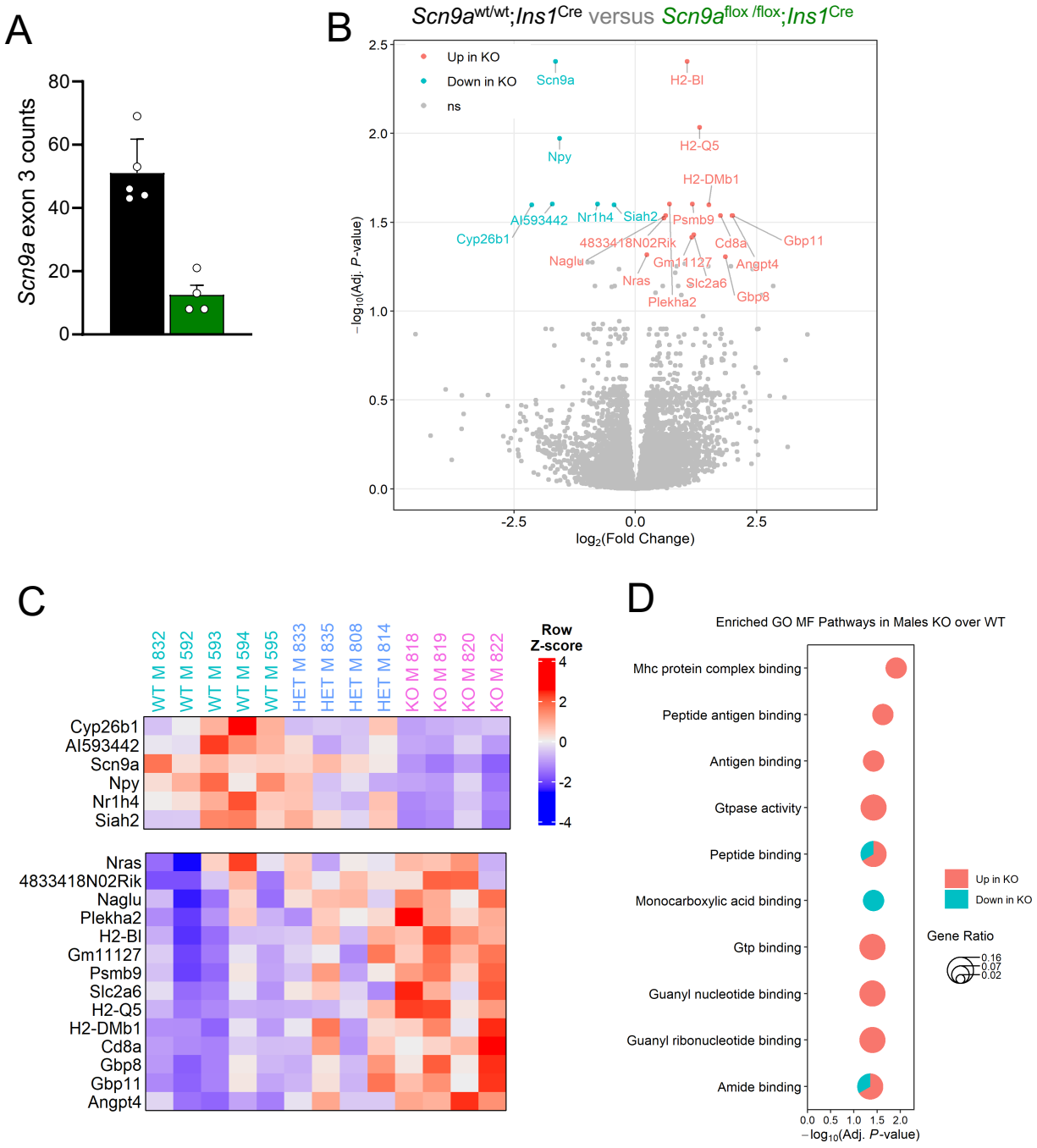
A
Scn9a exon 3 counts
80
60
40
20
0
B
Scn9awt/wt;Ins1Cre versus Scn9aflox /flox;Ins1Cre
Up in KO
Down in KO
ns
Scn9a
H2-Bl
H2-Q5
Npy
H2-DMb1
AI593442
Nr1h4
Siah2
Psmb9
Cyp26b1
4833418N02Rik
Cd8a
Gbp11
Naglu
Gm11127
Angpt4
Nras
Slc2a6
Plekha2
Gbp8
−log10(Adj. P-value)
log2(Fold Change)
C
WT M 832
WT M 592
WT M 593
WT M 594
WT M 595
HET M 833
HET M 835
HET M 808
HET M 814
KO M 818
KO M 819
KO M 820
KO M 822
Row Z-score
Cyp26b1
AI593442
Scn9a
Npy
Nr1h4
Siah2
Nras
4833418N02Rik
Naglu
Plekha2
H2-Bl
Gm11127
Psmb9
Slc2a6
H2-Q5
H2-DMb1
Cd8a
Gbp8
Gbp11
Angpt4
D
Enriched GO MF Pathways in Males KO over WT
Mhc protein complex binding
Peptide antigen binding
Antigen binding
Gtpase activity
Peptide binding
Monocarboxylic acid binding
Gtp binding
Guanyl nucleotide binding
Guanyl ribonucleotide binding
Amide binding
Up in KO
Down in KO
Gene Ratio
−log10(Adj. P-value)